	Fe
0.46	C
1.0	Cr
1.0	Mo
0.55	Ni

D6A
D6AC

GENERAL

D6AC is a quench-hardenable medium carbon low alloy steel. It is very similar to other popular grades such as Types 4340 and 4140, but has higher molybdenum content. The higher molybdenum content improves its hardenability, which is superior to that of 4340 steel. Tensile strength can be varied from about 90 to 300 ksi by changing the tempering temperature. Fracture toughness tends to decrease with increasing tensile strength but can also vary considerably at a given value of tensile strength. Fracture toughness has been found to be highly dependent on the quenching rate from the austenitizing or ausbay temperature. A high quench rate is required for high fracture toughness.

D6AC is susceptible to stress-corrosion cracking and to corrosion fatigue in moist and in aqueous environments, especially when tempered to high strength levels. The susceptibility is comparable to that of 300 M steels heat treated to similar strength levels. Weldability is good using the GTA process if proper procedures are followed. Although originally developed for hot die applications, D6AC is currently used extensively in aerospace applications requiring yield strength in the 215 ksi range combined with good fracture toughness. These applications include high performance aircraft structures, such as carry-through support structures, and the space shuttle solid rocket booster casings.

1.01 **Commercial Designations**
D6A (air melt), D6AC (consumable electrode vacuum melt).

1.02 **Alternate Designations**
UNS K24728, UNS K24729.

1.03 **Specifications**

1.031 AMS specifications, Table 1.031.

1.032 Other specifications: ASTM A579, MIL-S-8949, MIL-S-47036.

1.04 **Composition**

1.041 Composition, Table 1.041.

1.05 **Heat Treatment**

1.051 General. The heat treatment of D6AC is based on conventional quench and temper procedures in which sufficiently rapid cooling from the austenitizing (or ausbay) temperature produces a high strength martensitic structure which can be tempered to a wide range of strength levels. As commonly observed with low alloy high strength steels, the tensile strength decreases with increasing tempering temperature accompanied by an increase in the tensile ductility and in fracture toughness. However, variations in the austenitizing temperature and in the quench rate are capable of producing substantial changes in plane strain fracture toughness without appreciably affecting the tensile properties. These effects of heat treatment are discussed in Section 3.02721, which relates them to the microstructure. The achievement of a high level of tensile strength coupled with adequate fracture toughness requires special heat treating procedures and careful control, particularly for complex parts and heavy sections. Some examples are given below.

Ausbay quenching has the advantage of reducing thermal gradients and consequent distortion but increases production costs. Salt quenching from the austenitizing temperature (martempering) also reduces thermal gradients and minimizes quench cracking as compared with oil or water quenching. However, depending on section size and salt temperature, the cooling rate between about 900 F and the M_S temperature (approximately 550 F) may be insufficient to avoid the formation of intermediate products (bainites) which can reduce the fracture toughness. A complicating factor is the exothermic reaction which accompanies the martensite formation and can under some circumstances (e.g., insufficient salt-to-metal mass ratio) result in a decreased cooling rate during conversion to martensite. As pointed out in Section 3.02721, the cooling rate during martensite formation appears to be critical in establishing the fracture toughness. It is for the above reasons that sections having thicknesses or diameters greater than 1 inch are often oil quenched.

Oil quenching should not result in cracking provided that drastic changes in section size and high stress concentrations are avoided. Snap tempering is often employed and is designed to eliminate delayed cracking sometimes observed following quenching. In some cases, distortions produced by quenching may be eliminated by a sizing operation during tempering.

1.052 Anneal, 1500 to 1550 F, cool at 50 F per hour max to 1000 F (4).

1.053 Normalize, 1600 to 1750 F, air cool (29).

1.054 AMS conventional quench and temper procedures, Table 1.054.

1.055 Special quench and temper procedures. Following are two examples of heat treatment schedules which produce superior combinations of tensile strength and fracture toughness.

1.0551 Complex heavy sections. The F-111 carry-through structure is an example of a complex part involving sections of various thicknesses and requiring minimum distortion as a result of heat treatment. The procedure developed (53) is as follows: austenitize for at least 30 minutes at 1700 F; cool to 1550 F and equalize; ausbay quench at greater than 6 F/minute to 975 F and hold for 2 hours maximum; quench into 140 F oil; snap temper at 400 F for 2 hours minimum; temper at 1000 to 1025 F for 2 hours minimum, air cool; and retemper at 1015 to 1060 F for 2 hours minimum, air cool. The final tempering temperature was adjusted to produce the target properties of 220 to 240 ksi ultimate tensile strength and 90 ksi $\sqrt{\text{in.}}$ fracture toughness.

1.0552 Thin sections. The space shuttle solid rocket booster case is an example of relatively thin sections (approximately 0.30 inch) which can be resized during tempering to remove distortions

	Fe
0.46	C
1.0	Cr
1.0	Mo
0.55	Ni

D6A
D6AC

introduced during quenching. The procedure used (70) is as follows: austenitize in a protective atmosphere at 1590 to 1640 F for 2.5 hours minimum; salt quench to 325 F maximum, hold for at least 15 minutes, air cool to 175 F maximum; snap temper within 2 hours at 310 to 345 F for at least 3 hours; and double temper at 1070 to 1115 F for 6 to 7 hours and air cool to 175 F maximum. The tempering temperature is selected to produce the target properties of F_{ty} = 180 ksi minimum, F_{tu} = 195 to 225 ksi and K_{Ic} = 90 ksi $\sqrt{in.}$ minimum. Tempering temperatures are held to within ±10 F.

1.056 Stress relief, 1100 to 1200 F depending on the application.

1.057 Marstrain. Application of a small plastic strain after a relatively low temperature temper followed by a second low temperature temper can increase the tensile strength but reduces tensile ductility and crack strength (see Figures 3.02122 and 3.027112).

1.06 **Hardness**

1.061 End quench hardenability, Figure 1.061.

1.062 Effect of stress relief on hardness of cold worked sheet, Figure 1.062.

1.063 Effect of tempering temperatures on hardness, Figure 1.063.

1.064 Effect of austenitizing temperature on hardness, Figure 1.064.

1.07 **Forms and Conditions Available**

Sheet, bar, forging stock, tubing. Extrusions on special order.

1.08 **Melting and Casting Practice**

Electric furnace air melt is available but alloy is generally consumable electrode vacuum remelted or AOD/VAR melted.

1.09 **Special Considerations**

1.091 Fracture toughness is highly dependent on heat treatment conditions and can vary significantly independently of strength properties. See Sections 1.05 and 3.02721.

1.092 D6AC is subject to stress corrosion and corrosion fatigue in moist or aqueous environments. Crack-growth rates are increased by one order of magnitude or more in these environments as compared to rates in dry air or vacuum. Inhibitors such as sodium nitrite plus sodium borate effectively eliminate the environmental enhancement of crack-growth rates. Increased tempering time may also reduce susceptibility to stress corrosion. (See Section 2.032.)

1.093 Decarburizing should be avoided by use of suitable furnace atmospheres. (See 4340.)

2 PHYSICAL PROPERTIES AND ENVIRONMENTAL EFFECTS

2.01 **Thermal Properties**

2.011 Melting range, approximately 2740 F.

2.012 Phase changes.

2.0121 Time-temperature-transformation diagram, Figure 2.0121.

2.013 Thermal conductivity.

2.014 Thermal expansion, Figure 2.014.

2.015 Specific heat.

2.016 Thermal diffusivity.

2.02 **Other Physical Properties**

2.021 Density, 0.284 lb/in.^{3}, 7.87 gr/cm^3 (4).

2.022 Electrical properties.

2.023 Magnetic properties, ferromagnetic.

2.024 Emittance.

2.025 Damping capacity.

2.03 **Chemical Environments**

2.031 General corrosion.

2.0311 The potential-pH (Pourbaix) corrosion diagram for D6AC in an aqueous solution of 0.1M NaCl is shown in Figure 2.0312. General corrosion occurs at low pH values at potentials above -0.77 volt (standard calomel electrode). At lower potentials, no corrosion occurs. In the passive region, a protective film forms. This region contains two areas: an area of imperfect passivation where preexisting pits can grow, and an area of perfect passivation where these pits cannot grow (55, 56).

2.0312 Pourbaix diagram for corrosion of D6AC in 0.1M NaCl, Figure 2.0312.

2.032 Stress corrosion.

2.0321 D6AC is susceptible to stress-corrosion cracking and corrosion fatigue in moist and in aqueous environments. Variables affecting stress corrosion behavior include tempering temperature and time, specimen orientation, and the presence or absence of chemical inhibitors.

The effects of tempering temperature on the stress-corrosion crack-growth rates in distilled water and in H_2S are shown in Figure 2.0322. Lowest subcritical crack-growth rates in both water and H_2S are observed for material tempered at 1000 F. This material has the highest fracture toughness and lowest tensile strength. Conversely, the highest crack-growth rates are observed for material tempered at 400 F, which has the lowest fracture toughness and highest tensile strength. Crack propagation in H_2S is transgranular, while it is intergranular in non-sulfide aqueous environments (57).

2.0322 Effects of tempering temperature on stress-corrosion crack-growth behavior in water and in hydrogen sulfide, Figure 2.0322.

2.0323 The susceptibility of D6AC to stress-corrosion cracking is anisotropic when the microstructure is banded. Banded microstructure, characterized by alternate layers of solute-rich and solute-depleted layers, is common and results from standard fabrication and heat treatment procedures. As shown in Figure 2.0324 for material in the 2 hr/1020 F tempered condition, crack-growth rates in both distilled water and in hydrogen are about 10-fold greater for the S-L orientation than for the T-L orientation. These differences reflect the greater susceptibility of solute-rich bands (which

Fe	
0.46	C
1.0	Cr
1.0	Mo
0.55	Ni

D6A
D6AC

are more favorably oriented for corrosion in the S-L specimens) to intergranular crack growth as compared with solute-depleted bands. However, crack-growth rates can be reduced by nearly two orders of magnitude and the threshold stress intensity almost doubled by increasing the tempering time at 1020 F from 2 hours to 200 hours. This improvement, shown in Figure 2.0325, is achieved without loss in tensile strength or fracture toughness. The fracture path is also changed from intergranular to transgranular on increasing the tempering time. These improvements are attributed to increased precipitation of Mo_3P and decreased grain boundary segregation of molybdenum and phosphorus with increasing tempering time (58).

2.0324 Effects of orientation on subcritical stress-corrosion crack-growth behavior in distilled water and in hydrogen, Figure 2.0324.

2.0325 Effect of tempering time at 1020 F on subcritical stress-corrosion crack-growth behavior in distilled water, Figure 2.0325.

2.0326 The environmental enhancement of crack-growth rates under static sustained load or low cycle fatigue conditions can be minimized or eliminated through the use of chemical inhibitors. As shown in Figures 2.0327 and 2.0328, the stress-corrosion and corrosion fatigue crack-growth rates in an aqueous solution of 0.1M NaCl are significantly reduced by the addition of an inhibitor consisting of 0.1M $NaNO_2$ plus 0.1M $Na_2B_4O_7$ (59). This inhibitor system lowers crack-growth rates by one-half to one order of magnitude to rates substantially identical to those observed in ambient air (60). This inhibitor combination is equally effective in the presence or absence of sodium chloride. In the absence of inhibitors, distilled water is slightly more aggressive than sodium chloride solutions in accelerating crack-growth rates (60). Hydrazine is also effective in reducing the stress-corrosion crack-growth rate in 0.1M NaCl and nil chloride solutions. Inhibition of crack growth is related to the formation of nitride ion which prevents hydrogen evolution at the crack tip. Sodium dichromate (0.1M $Na_2Cr_2O_7$) inhibits crack growth in nil chloride solutions but is ineffective in chloride solutions (60, 61). Corrosion inhibitors also increase the value of K_{Iscc}. This is of potential practical importance since the critical flaw size varies as the square of K_{Iscc}. Increasing the critical flaw size improves the ease with which such flaws can be detected by nondestructive methods (62).

2.0327 Effects of inhibitors on stress-corrosion crack-growth behavior, Figure 2.0327.

2.0328 Effects of inhibitors on corrosion fatigue crack-growth behavior, Figure 2.0328.

2.0329 Accelerated corrosion under static or dynamic stress conditions is attributed to localized hydrogen embrittlement at propagating crack tips. Measurements of local pH at advancing crack tips indicate that the crack tips are acidified with respect to the bulk corrodent solutions (such as distilled water or aqueous NaCl solutions). Hydrogen analyses of local areas of fracture surfaces also indicate increased hydrogen contents after corrosion in aggressive environments. In contrast, the addition of an oxidizing inhibitor such as hydrazine to distilled water or a salt solution causes the pH and the potential at the crack tip to remain the same as in the bulk solution and therefore unfavorable for hydrogen evolution. Local hydrogen analyses confirm that hydrogen contents remain at a low level near the crack tip under these conditions (62).

2.03210 The apparent incubation time for subcritical crack growth under stress corrosion conditions tends to decrease with decreasing stress intensity on initial loading, as shown in Figure 2.03211. Unfortunately, the scatter in these data precludes the derivation of a definitive relationship between incubation time and applied stress intensity. It has been suggested that the incubation period may be a function of the ratio of the applied stress intensity at experimental load conditions to that employed during fatigue precracking (63). Incubation time also varies with the sensitivity of the device used to detect cracking, further complicating the understanding of its relation to other factors.

Crack arrest periods and changes in crack propagation rates have also been observed following load-shedding. The period of crack arrest and the crack-growth rate following crack arrest vary with the amount of load shed and the original applied stress intensity. The greater the amount of load shed, the longer is the crack arrest period, and the higher the original applied stress intensity, the shorter is the crack arrest period for the same amount of load shedding. The crack-growth rates following crack arrest are lower following greater increments of load shedding. However, as for incubation times following initial load application, the apparent crack arrest times and changes in crack propagation rates vary in a complex manner with prior load history. Definitive relationships have yet to be established. It does appear that prestressing retards stress-corrosion cracking and is therefore beneficial (63, 64).

2.03211 Incubation times for stress-corrosion crack-growth initiation in aqueous solutions as a function of initial stress intensity factor, Figure 2.03211.

2.033 Mercury corrosion.

2.0331 Stress-corrosion crack-growth behavior in liquid mercury and low pressure hydrogen environments, Figure 2.0331.

2.034 Hydrogen environment effects. (See Figures 2.0324, 2.0331, and 3.0516.)

3 MECHANICAL PROPERTIES

3.01 Specified Mechanical Properties

3.011 AMS specified mechanical properties, Table 3.011.

3.02 Mechanical Properties at Room Temperature

3.021 Tension – stress-strain diagrams – tension properties.

3.0211 Stress-strain diagrams.

3.02111 D6AC exhibits cyclic softening in the quenched and tempered condition, as shown in Figure 3.02112a and b. This cyclic softening results in an 18 percent decrease in yield strength under cyclic,

	Fe
0.46	C
1.0	Cr
1.0	Mo
0.55	Ni

D6A
D6AC

as compared to monotonic, conditions. This reduction in yield strength can occur during design life as a result of cyclic loading and should be considered by the designer as the performance of components can be impaired.

Cyclic softening has been related to the monotonic work hardening exponent n, with small values indicating a propensity for cyclic softening. Low n values reflect minimal work hardening and a starting microstructure which is optimally strengthened. The values of n for D6AC for the two heat treatments (Figure 3.02112a and b) are quite low, 0.03 and 0.02, respectively, and are consistent with the observed cyclic softening. Strength-differential effects between tension and compression are also exhibited by D6AC, but these effects are smaller than the cyclic softening effect. In monotonic loading, the flow stress is greater in compression than in tension, while the opposite occurs during cyclic loading (52).

3.02112 Monotonic and cyclic stress-strain curves for two different heat treatments [(a) 2-hour temper and (b) 4-hour temper], Figure 3.02112.

3.02113 Effects of tempering temperature on stress-strain curves at room temperature, Figure 3.02113.

3.0212 Tensile properties for sheet.

3.02121 Effect of tempering temperature on tensile properties of sheet, Figure 3.02121.

3.02122 Effect of marstrain on tensile properties of sheet, Figure 3.02122.

3.02123 Effect of low carbon content and various tempering temperatures on tensile properties of sheet, Figure 3.02123.

3.02124 Effect of tempering temperature on tensile properties at two austenitizing temperatures, Figure 3.02124.

3.02125 Effect of tempering temperature on tensile properties of air and vacuum melt alloy sheet, Figure 3.02125.

3.0213 Tensile properties for plate.

3.02131 Effect of tempering temperature on tensile properties of plate, Figure 3.02131.

3.02132 Range of tensile properties in plates tempered at 500 to 550 F, Table 3.02132.

3.02133 Effect of austempering temperature on tensile properties of plate, Figure 3.02133.

3.0214 Tensile properties for bar.

3.02141 Effect of tempering temperature on tensile properties of bar, Figure 3.02141.

3.02142 Effect of tempering temperature on tensile properties of strain-aged bar, Figure 3.02142.

3.0215 Tensile properties for forgings.

3.02151 Effect of tempering temperature on tensile properties of rolled ring forgings, Figure 3.02151.

3.02152 Effect of forging reduction on tensile properties of a variable-cross-section ausformed forging tempered at 500 F, Figure 3.02152.

3.02153 Effect of forging reduction on tensile properties of a variable-cross-section ausformed forging tempered at 900 F, Figure 3.02153.

3.02154 Effect of forging and tempering temperature on tensile properties of ausformed forgings, Figure 3.02154.

3.02155 Effect of shot peening and tempering temperature on tensile properties, Figure 3.02155.

3.02156 Effect of tempering temperature on tensile properties for three thermal mechanical processing treatments of forged alloy, Figure 3.02156.

3.0216 Tensile properties of extrusions.

3.02161 Tensile properties of extrusion at two tempering temperatures, Table 3.02161.

3.0217 Tensile properties of shear spun alloy.

3.02171 Effect of tempering temperature on tensile properties of shear spun alloy, Figure 3.02171.

3.02172 Effect of shear form reduction on tensile properties, Figure 3.02172.

3.022 Compression – stress-strain diagrams – compression properties.

3.0221 Compression stress-strain diagrams, see Section 3.0211.

3.023 Impact (see also Section 3.033).

3.0231 Effect of tempering temperature on impact properties, Figure 3.0231.

3.024 Bending.

3.025 Torsion and shear.

3.0251 Effect of shear form reduction on shear strength, Figure 3.0251.

3.026 Bearing.

3.027 Stress concentration.

3.0271 Notch properties. (See also Section 3.0272.)

3.02711 Notch properties for sheet.

3.027111 Effect of tempering temperature on sharp notch properties of sheet, Figure 3.027111.

3.027112 Effect of marstrain on sharp notch properties of sheet, Figure 3.027112.

3.027113 Effect of tempering temperature on sharp notch properties of air and vacuum melt sheet, Figure 3.027113.

3.027114 Effect of low carbon content and tempering temperature on sharp notch strength of sheet, Figure 3.027114.

3.027115 Effect of notch root radii on sharp notch strength of sheet, Figure 3.027115.

3.02712 Notch properties of plate.

3.027121 Effect of crack length on crack strength of three thicknesses of plate each from a different heat, Figure 3.027121.

3.027122 Effect of surface cracks on crack strength of plate at strength levels between F_{ty} = 190 and 215 ksi, Figure 3.027122.

3.02713 Notch properties for bar.

3.027131 Effect of tempering temperature on notch and smooth tensile properties of bar, Figure 3.027131.

3.027132 Effect of tempering temperature on the sharp notch strength of bar, Figure 3.027132.

3.02714 Notch properties for forgings.

3.027141 Effect of surface cracks on crack strength of forging, Figure 3.027141.

3.02715 Effect of tempering temperature on sharp notch properties of shear spun alloy, Figure 3.02715.

3.02716 Effect of surface cracks on burst strength of thin walled cylinders, Figure 3.02716.

3.0272 Fracture toughness. (See also Section 3.0372.)

3.02721 General. The fracture toughness of D6AC is highly dependent on heat treatment variables, as discussed in Section 1.05. Results from a fracture toughness study in support of the F-111 aircraft wing pivot support structure (carry-through box) are shown in Figure 3.02722 and Tables 3.02723, 3.02724, 3.02725, and 3.02726. Additional data from a separate program on heat treatment effects

	Fe
0.46	C
1.0	Cr
1.0	Mo
0.55	Ni

D6A
D6AC

are presented in Table 3.02727. These studies indicate that D6AC can be heat treated to give similar tensile properties but with fracture toughness values differing by a factor of more than 3.

An increase in toughness associated with increasing austenitizing temperature (Figure 3.02722) has also been observed in 4340 tempered at 400 F (71). In this case, the beneficial effect from increasing the austenitization temperature was attributed to increasing solution of second phase void nucleating particles (carbide particles and sulfide inclusions), which resulted in larger void spacings and consequent increased energy absorption by plastic flow during fracture.

The variation in fracture toughness associated with changes in the quenching rate are illustrated in Table 3.02727. These data relate to quenching an 0.75-inch thick section from an ausbay temperature of 970 F, but similar effects would be expected for direct quenching from the austenitizing temperature. Focusing on an austenitizing temperature of 1700 F and a tempering temperature of 1020 F, it is evident that oil quenching gives the highest toughness (94.2 ksi $\sqrt{in.}$). Salt quenching at 365 F gives a toughness of 88 ksi $\sqrt{in.}$, while salt quenching at 410 F or air cooling both give lower toughnesses. It should be noted that tensile strength properties vary insignificantly for these quenching conditions.

It has been suggested (66) that these changes in fracture toughness with quenching rate are related to the nature of the as-quenched martensite structure. High toughness values are obtained after tempering micro-twinned plate martensite, which predominates after oil quenching. Low toughness values are obtained after tempering lath-type martensite, which predominates after air cooling and is associated with a bainitic form of carbide precipitation.

3.02722 Effects of austenitizing temperature and quench medium on fracture toughness, Figure 3.02722.
3.02723 Plane strain fracture toughness of 0.8-inch thick CVM plate, Table 3.02723.
3.02724 Plane strain fracture toughness of CVM forgings, Table 3.02724.
3.02725 Plane strain fracture toughness of plate and forged parts, Table 3.02725.
3.02726 Effects of heat treatment on fracture toughness of plate, forgings, and billets at room temperature, Table 3.02726.
3.02727 Effects of heat treatment on fracture toughness of bar, Table 3.02727.
3.02728 The majority of plane strain fracture toughness data reported apply to yield strength levels below 220 ksi. However, a limited amount of information from fatigue-cracked cylindrical specimens (Figure 3.02729) indicates that the toughness drops rapidly with increasing strength level and that the highest strength conditions are relatively brittle.
3.02729 Effect of tempering temperature on sharp notch properties and fracture toughness of plate, Figure 3.02729.
3.027210 Effect of tempering temperature on fracture toughness and yield strength for three thermal-mechanical processing treatments of forged alloy, Figure 3.027210.
3.028 Combined properties.

3.03 **Mechanical Properties at Various Temperatures**
3.031 Tension – stress-strain diagrams – tension properties.
3.0311 Stress-strain curves for plate at room temperature and 250 F, Figure 3.0311.
3.0312 Effect of test temperature on tensile properties of bar at several strength levels, Figure 3.0312.
3.0313 Effect of test temperature on tensile properties of bar, Figure 3.0313.
3.0314 Effect of test temperature on tensile properties of plate, Table 3.0314.
3.0315 Effect of test temperature on tensile properties of forgings, Table 3.0315.
3.032 Compression – stress-strain diagrams – compression properties.
3.033 Impact.
3.0331 Elevated temperature Charpy V-notch impact properties, Figure 3.0331.
3.0332 Elevated temperature Charpy U-notch impact properties for various strength levels, Figure 3.0332.
3.0333 Low temperature Charpy V-notch impact properties, Figure 3.0333.
3.0334 Effect of test temperature on impact strength of a variable cross section ausformed forging, Figure 3.0334.
3.034 Bending
3.035 Torsion and shear.
3.036 Bearing.
3.037 Stress concentration.
3.0371 Notch properties.
3.0372 Fracture toughness.
3.03721 Effect of test temperature on plane strain fracture toughness of 0.8-inch thick CVM plate, Figure 3.03721.
3.03722 Effect of test temperature on plane strain fracture toughness of 1.5 to 1.8-inch thick CVM plate, Figure 3.03722.
3.03723 Effect of test temperature on plane strain fracture toughness of CVM forgings, Figure 3.03723.
3.038 Combined properties.

3.04 **Creep and Creep-Rupture Properties**
3.041 Creep-rupture curves at 900 and 1000 F, Figure 3.041.
3.042 Creep-rupture strength of smooth and notched bar at elevated temperatures, Figure 3.042.

3.05 **Fatigue Properties**
3.051 Fatigue strength of marstrained sheet, Table 3.051.
3.052 Effect of test temperature on smooth and notched fatigue properties of bar, Table 3.052.
3.053 Low cycle fatigue behavior of cracked plate specimens and tanks, Figure 3.053.
3.054 S-N curves for 220 to 240 ksi hot rolled plate, Figure 3.054.
3.055 S-N curves for 260 to 280 ksi forged bar, Figure 3.055.
3.056 Effects of humidity on fatigue behavior of keyhole notched bar at 95 F, Figure 3.056.

	Fe
0.46	C
1.0	Cr
1.0	Mo
0.55	Ni

D6A
D6AC

3.057 The fatigue crack-growth behavior for materials quenched and tempered to two different strength levels and four different fracture toughness levels is shown in Figure 3.058. In the central portions of these curves, the fatigue crack-growth rates are proportional to $\Delta K^{2.4}$ and are independent of fracture toughness for toughness values ranging from 42 to 91 ksi $\sqrt{in.}$ at essentially the same tensile strength. Variations in yield and ultimate strength have no significant effect on the rate of fatigue crack growth in the range where da/dN is proportional to $\Delta K^{2.4}$. At ΔK values greater than $0.7K_{Ic}$, void coalescence and microcleavage cause progressively accelerated crack growth as the fracture toughness is approached (68). Data from the F-111 program, shown in Figure 3.059, are in agreement with data in Figure 3.058.

3.058 Effects of quenching on fatigue crack-growth behavior in dry air at room temperature, Figure 3.058.

3.059 Fatigue crack-growth rates for high and medium toughness plate in desiccated air at room temperature, Figure 3.059.

3.0510 Figures 3.0511 through 3.0514 illustrate the fact that water, which is almost always present in service environments, constitutes an aggressive environment under conditions of cyclic loading. The rate of crack growth is not influenced by the presence of water vapor or water at a cyclic frequency of 600 cpm, as shown in Figure 3.0511a. However, when the frequency is reduced to 60 cpm, moisture clearly increases the rate of crack growth, as shown in Figure 3.0511b.

Moderate humidity, distilled water, and water-saturated JP-4 fuel environments all increase the fatigue crack-growth rate at low frequency (6 cpm), as shown in Figures 3.0512, 3.0513, and 3.0514, respectively. The change in frequency and sensitivity to moisture are also associated with a change in fracture mode from transgranular at the higher frequency to intergranular at the lower frequency (69).

3.0511 Effects of humidity and frequency on fatigue crack-growth behavior at room temperature [(a) frequency 600 cycles/minute and (b) frequency 60 cycles/minute], Figure 3.0511.

3.0512 Fatigue crack-growth rates for medium toughness plate in laboratory air (50 to 70 percent RH) at room temperature, Figure 3.0512.

3.0513 Fatigue crack-growth rates for high and medium toughness plate in distilled water at room temperature, Figure 3.0513.

3.0514 Fatigue crack-growth rates for high and medium toughness plate in water-saturated JP-4 fuel at room temperature, Figure 3.0514.

3.0515 Fatigue crack-growth rates in hydrogen are higher than those in dry air or vacuum, as shown in Figure 3.0516. The rates in hydrogen are also frequency dependent, with lowest frequencies giving the highest crack-growth rates. In contrast, the crack-growth rates in dry air or in vacuum are much less frequency dependent (over the range 3 to 60 cpm). The crack-growth rates in hydrogen are proportional to the duration of the maximum stress intensity during each loading cycle for the square wave illustrated in Figure 3.0512. For wave forms such as triangular, positive sawtooth, and negative sawtooth (ratios of loading to unloading times of 1:1, 10:1, and 1:10, respectively), the crack-growth rates are proportional to the duration of the loading portion of the cycle (65).

3.0516 Effects of cyclic frequency on fatigue crack-growth behavior in hydrogen with comparison to air and vacuum, Figure 3.0516.

3.06 **Elastic Properties**

3.061 Poisson's ratio.

3.062 Modulus of elasticity.

3.0621 Modulus of elasticity at room and elevated temperatures, Figure 3.0621.

3.063 Modulus of rigidity.

3.064 Tangent modulus.

3.065 Secant modulus.

4 FABRICATION

4.01 **Forming**

4.011 Forging. Starting temperature 2250 F maximum, finishing temperature 1800 F minimum. Slow cool after finishing. Alternately hold at 1200 F, 12 hours immediately following forging, raise temperature to 1650 F and then cool to 1200 F, hold 10 hours and air cool.

4.02 **Machining and Grinding**

Properties are similar to those of Type 4340, Code 1206.

4.03 **Joining**

4.031 General. This alloy is weldable in sheet and heavy sections. Extensive experience is available in the welding of pressure vessels having section thickness between 0.2 and 1.0 inch (5, 22), heat treated to yield strength levels between 180 and 215 ksi. For critical applications the GTA process is preferred using vacuum melted wires of lower carbon content than the parent metal and containing minimum amounts of P, S, and gases. Welds made in this manner will have a higher toughness but a somewhat lower yield strength than the parent plate. If tempering temperatures above about 1125 F are employed 17-22A (S) (AMS 6458) weld wire has been used. This substitution improves weld strength for the higher tempering temperatures (5). Using proper techniques, primary weld efficiencies after heat treatment approach 100 percent. Preheat and a postheat immediately following welding are necessary to avoid cracking (see Table 4.0311). The toughness of primary GTA welds heat treated to yield strength levels less than about 200 ksi is essentially equal to that of the parent metal (see Figure 4.0312). Weld repair following heat treatment requires special precautions (see Table 4.0311) and results in some loss in strength and toughness (see Figure 4.0312) (4, 5, 22).

4.0311 Recommended weld heat treat sequence for primary welds and weld repair after heat treatment, Table 4.0311.

4.0312 Effect of surface crack size on sharp notch strength of primary welds and weld repairs made after heat treatment, Figure 4.0312.

4.0313 Effect of welding on low temperature Charpy V impact properties, Figure 4.0313.

4.0314 Hardness survey on welded plate, Figure 4.0314.

4.09 **Surface Treating**
(See 4340, Code 1206.)

REFERENCES

1 Henning, H. J. and Boulger, F. W., "High Strength Steel Forgings", DMIC Report 143 (January 5, 1961).

2 Kaiser Fleetwings, Inc., "Final Report on the Effect of Stress Relief vs a Normalize and Temper Treatment on the Final Mechanical Properties of AMS 6434, Ladish D6A, X2 (Modified 4137)" (November 1960).

3 Kennedy, E. M., Jr., "The Status of Research and Development for High Strength Aircraft Steels", WADC TN 59-326 (July 1960).

4 Ladish Co., "Ladish D6A, High Strength Steel" (October 4, 1957) (1963).

5 Private Communication, G. R. Sipple, General Motors Allison Division with W. F. Brown, Jr. (1965).

6 Brown, W. F., Jr., Personal Communication, NASA Unpublished Data (1960).

7 Check, S. V., "Progress Report on Slow Crack Extension and Low Cycle Fatigue of Ladish D6AC at 240,000 psi Yield Strength Level", U.S. Naval Weapons Plant, Technical Memo 169 (September 1961).

8 Hanink, D. K., Personal Communication, General Motors Allison Division (November 1961).

9 David, C. K., Personal Communication, Ladish Co. (January 15, 1962).

10 Martin, C. F., Williams, A. J., and Gerberich, W. W., "Effects of Deformation of the Metastable Austenitic Condition on the Properties of High Strength Steel Forgings", Aeronutronic Division, Philco Corp., ASK-TDR 63-836, ASD Contract AF33(657)-8539 (September 1963).

11 Yount, R. E., "Determination of Engineering Properties of Marstrained Steels", General Electric, Evandale, Ohio, ASD-TDR-62-230, ASD Contract AF33(616)-7655 (August 1962).

12 Davis, S. O., "Elevated Temperature Fatigue Properties of D6AC High Strength Steel", ASD-TDR-63-645 (October 1963).

13 Carmen, C. M. and Mulherin, J. H., "Low Cycle Fatigue Characteristics of Ultra High Strength Steels", Frankford Arsenal Report R-1707 (February 1964).

14 Pratt, W. W., "Material Evaluation of D6AC Steel Extrusion Mechanical and Metallurgical Properties", General Dynamics, Fort Worth, Test Data Memo FTDM 3234, ASD Contract AF33(657)-11214 (April 15, 1964).

15 Bhat, G. K., "A Study of the Behavior of Small Pressure Vessels Under Biaxial Stress Conditions and in Presence of Surface Cracks", Mellon Institute, NRL Contract NOnr-3764(00)(X) (June 25, 1963).

16 Carmen, C. M., Armiento, D. F., and Markus, H., "Plane Strain Fracture Toughness Measurements of High Strength Steels", ASME Journal of Basic Engineering (March 1963).

17 Terry, E. L. and McClaren, S. W., "Biaxial Stress and Strain Data on High Strength Alloys for Design of Pressurized Components", Chance-Vought Corp., ASD-TDR-62-401, ASD Contract AF33(616)-7720 (July 1962).

18 Tiffany, C. F. and Lorenz, P. M., "An Investigation of Low Cycle Fatigue Failures Using Applied Fracture Mechanics", The Boeing Company, Aero-Space Division, ML-TDR 64-53, ASD Contract 33(657)-10251 (May 1964).

19 Check, S. V., "Toughness, Slow Crack Extension and Low Cycle Fatigue of Ladish D6AC at 24,000 psi, Y.S. Level", U.S. Naval Weapons Plant, Technical Memo No. 169, NRL-Project 62ROS-19A (September 26, 1961).

20 Urban, R. J., "Plane Strain Fracture Toughness of Large D6AC Steel Specimens Heat Treated to 220–240 and 260–280 ksi Strength Level", General Dynamics, Fort Worth, Test Data Memo FTDM-3178, ASD Contract AF33(657)-11214 (April 15, 1964).

21 Urban, R. J., "Plane Strain Fracture Toughness of Large D6AC Steel Specimens", General Dynamics, Fort Worth, Report FGT3064, ASD Contract AF33(657)-8260-1 (November 1, 1963).

22 Mehra, Y., "Mechanical and Fracture Toughness Properties of D6AC Post Heat Treat Weld Repair", Curtiss Wright Corp., Wright Aero Division (October 23, 1964).

23 Betner, D. C., "Effect of Section Thickness and Partial Thickness Crack Size on Gross Strength of D6AC Steel at Ultimate Strength Level of 215 ksi", Allison Materials Research Laboratory, Report 62M23 (September 21, 1962).

24 Green, R. B., "Evaluation of D6AC and 18-Ni-Co-Mo-High Strength Steel Plate for Heavy Wall Large Diameter Rocket Motor Case Applications", Allison Materials Research Laboratories, Report No. 62M34 (June 7, 1963).

25 Wessel, E. T., Hovan, R. P., and Pryle, W. H., "Preliminary Evaluation of the Fracture Characteristics of D6AC Rocket Motor Cases", Westinghouse Research Laboratories, Research Report 63-848-307-R1 (August 27, 1963).

26 Haese, W. P. and Masters, J. N., "An Evaluation of Large Diameter Solid Propellant Motor Case Materials", The Boeing Company, Report No. 02-22314M (May 22, 1963).

27 Crucible Steel Company, "Data Sheet for Crucible D6", Issue No. 2 (1965).

28 AMS 6431F (January 15, 1980).

29 AMS 6438C (July 1, 1981).

30 Excelo Developments, Inc., "Investigation and Evaluation of High Strength Steels in Heavy Gauges for Large Diameter Solid Propellant Rocket Engine Cases", Mellon Institute, AF Contract No. AF04(611)-8517 (January 1963).

31 "Evaluation of Low Carbon Ladish D6AC Steel", Aerojet General Corporation, Report No. 278, Contract No. AF33(657)-8890 (September 1962).

32 Vazquez, A. J., "Developing a Process for Ausforming Large, High Strength Steel Aircraft

	Fe
0.46	C
1.0	Cr
1.0	Mo
0.55	Ni

D6A
D6AC

	Fe
0.46	C
1.0	Cr
1.0	Mo
0.55	Ni

D6A
D6AC

Structural Components With Improved Design and Weight Reduction", Report IV, IR-8-354, Ladish Company (July 1966).

33 Jacobs, F., "Mechanical Properties of Materials Fabricated by Shear Forming", T.D.R. ASD-TDR-62-830, Contract AF33(616)-7874, Temco Electronics and Missiles Company (February 1963).

34 Weiss, V., Nash, G., and Schroder, K., "Crack Initiation in Metallic Materials", Syracuse University Research Institute, Contract NOw-64-0265-d (March 1965).

35 Smith, H. R., "Evaluation of Ladish D6AC Steel", Aerojet General Corporation, Contract AF33(657)-8890 (January 1963).

36 Davish, R. C. and Crownover, W. S., "A Comparison of the Toughness Characteristics of D6 Air and Vacuum Melt Material", Army Missile Command, DA Project LB 222901A205 AMC RA RK TR 64 11 (March 1964).

37 Amateau, M. F. and Steigerwald, E. A., "Fracture Characteristics of Structural Metals", Contract NOw-64-0186C (January 1965).

38 Albom, J. J., "Brazing of Ultra High Strength Steel", Aerojet General Corporation, Contract No. AF33(657)-8890 (January 1963).

39 Faulker, J. M., Hanna, G. L., and Peck, J. V., "Development of Welding Procedures and Filler Materials for Joining High Strength Low Alloy Steels", TRW Inc., Contract AF33(657)-11229 (September 1965).

40 Robinson, R. B. and Uzdarwin, R. J., "Investigation of Stress Corrosion Cracking of High Strength Alloys", Aerojet General Corporation, Contract DA-04-495-ORD-3069, Report 2092 (August 1961).

41 Hartbower, C. E., Gerberich, W. W., and Crimmins, P. P., "Characterization of Fatigue Crack Growth by Stress-Wave Emission", Contract NAS-1-4902, Aerojet General Corporation, Sacramento, California (June 1966).

42 Ault, R. T., McDowell, K. O., and Hendricks, P. L., "Increased Reliability of a High Strength Steel Through Thermal Mechanical Treatments", AFML-TR-66-276 (September 1966).

43 Hartbower, C. E. and Orner, G. M., "Metallurgical Variables Affecting Fracture Toughness in High Strength Sheet Alloys", ASD-TDR-62-868 (June 1963).

44 Heitzmann, R. J., "Effect of Decarburization and Surface Defects on the Notched Fatigue Strength of Steel", ADR 02-09-67, Grumman Aircraft Engineering Corp., Advanced Development Program (April 1967).

45 Feddersen, C. E., Moon, D. P., and Hyler, W. S., "Crack Behavior in D6AC Steel – An Evaluation of Fracture Mechanics Data for the F-111 Aircraft", Metals and Ceramics Information Center, MCIC-72-04 (January 1972).

46 Wei, R. P., Novak, S. R., and Williams, D. P., "Some Important Considerations in the Development of Stress Corrosion Cracking Test Methods", Materials Research and Standards, ASTM Vol. 12 (September 1972), p 25.

47 Mulherin, J. H., "Stress Corrosion Susceptibility of High Strength Steel in Relation to Fracture Toughness", *Journal of Basic Engineering*, Trans. ASME Serial D, Vol. 88 (December 1966), pp 777–782.

48 Campbell, J. E., Berry, W. E., and Feddersen, C. E., "Damage Tolerant Design Handbook", Metals and Ceramics Information Center, HB-01 (December 1972).

49 Private Communication from C. Dale Little, General Dynamics Corporation, Convair Aerospace Division, Fort Worth to W. F. Brown, Jr. (1973).

50 AMS 5027B (July 1, 1984).

51 AMS 5028A (October 15, 1980).

52 Jones, W. B. and Swearengen, J. C., "Mechanical Stability of Ultrahigh Strength Steels", *Materials Science and Engineering*, Vol. 41, No. 2 (December 1979), pp 225–235.

53 Peterman, G. L. and Jones, R. L., "Effects of Quenching Variables on Fracture Toughness of D6AC Steel Aerospace Structures", *Metals Engineering Quarterly*, Vol. 15, No. 2 (May 1975), pp 59–64.

54 Ortiz, R. T., "Heat Treating Space Shuttle Parts to Fracture Toughness Specifications", *Metal Progress*, Vol. 111, No. 3 (March 1977), pp 54–55.

55 Parrish, P. A., Chen, C. M., and Verink, E. D., Jr., "Retardation of Crack Propagation for D6AC High-Strength, Low-Alloy Steel in Aqueous Media by Addition of Oxidizing Inhibitors", Stress Corrosion – New Approaches, ASTM STP 610 (1976), pp 189–198.

56 Verink, E. D., Jr., "Use of the Experimental Pourbaix Diagram for D6AC Steel to Interpret Its Corrosion Behavior in Aqueous Media", Florida University, Gainesville, AFML TR-76-8 (February 1976).

57 Cullen, W. H., "A Study of Hydrogen Sulfide Accelerated Stress-Corrosion Cracking in D6AC Steel", Naval Research Laboratory, Washington, D.C., NRL–MR-3200 (January 1976).

58 Pollock, W. J., Ryan, N. E., and Nankivell, J. F., "Relationship Between Banding and Susceptibility to Environment-Assisted Cracking in a Quenched and Tempered Low Alloy Steel", *Corrosion Science*, Vol. 22, No. 3 (1982), pp 215–229.

59 Bhansali, K., Lynch, C. T., Vahldiek, F., and Summitt, R., "Effect of Multifunctional Inhibitors on Crack Propagation Rates of High Strength Steel in Corrosive Environments", paper presented at International Conference on Effect of Hydrogen on Behavior of Materials, Moran, Wyoming (September 7–11, 1975).

60 Lynch, C. T., Vahldiek, F. W., and Thornton, F., "Comparison of Environmentally Enhanced Crack-Growth Rates of 1410 and Other High-Strength Steels", Proceedings of the 1978 Tri-Service Conference on Corrosion, New Orleans, Louisiana (October 4–6, 1978), pp 341–369.

61 Lynch, C. T., Bhansali, K. J., and Parrish, P. A., "Inhibition of Crack Propagation of High Strength Steels Through Single and Multifunctional Inhibitors", Air Force Materials Laboratory, Wright-Patterson AFB, Ohio, AFML-TR-76-120 (August 1976).

62 Parrish, P. A., Das, K. B., Chen, C. M., and Verink, E. D., Jr., "Inhibition of Hydrogen Embrittlement of D6AC Steel in Aqueous Oxidizing Media".

paper presented at International Conference on Effect of Hydrogen on Behavior of Materials, Moran, Wyoming (September 7–11, 1975).

63 Gilbreath, W. P. and Adamson, M. J., "Aqueous Stress-Corrosion Cracking of High-Toughness D6AC Steel", Stress Corrosion – New Approaches, ASTM STP 610 (1976), pp 176–187.

64 Noronha, P. J., "Kinetic Studies of the Stress Corrosion Cracking of D6AC Steel", NASA Marshall Space Flight Center, Huntsville, Alabama, NASA TM X-64923 (March 25, 1975).

65 Lynch, S. P. and Ryan, N. E., "Mechanisms of Hydrogen Embrittlement – Crack Growth in a Low-Alloy Ultra-High-Strength Steel Under Cyclic and Sustained Stresses in Gaseous Hydrogen", Aeronautical Research Labs, Melbourne, Australia, ARL/MAT-103 (May 1978).

66 Ryan, N. E., "Relationship Between Microstructure and Fracture Toughness in D6AC Steel", Aeronautical Research Labs, Melbourne, Australia, ARL/MET-NOTE–103 (April 1974).

67 Mann, J. Y. and Kemsley, D. S., "The Effects of Very Dry and Fully Water Saturated Air Environments on the Fatigue Life of D6AC Steel Under Constant and Variable Amplitude Loading Sequences", *Corrosion*, Vol. 35, No. 10 (October 1979), pp 465–471.

68 Ryan, N. E., "Fatigue-Crack Growth in D6AC Steel Heat-Treated to Different Values of Fracture Toughness", Aeronautical Research Labs, Melbourne, Australia, ARL/MAT-110 (April 1979).

69 Ryan, N. E., "Fatigue-Crack Growth and Fracture in D6AC Steel", Aeronautical Research Labs, Melbourne, Australia, ARL/MAT-368 (September 1976).

70 Specification STW7-2608, Wasatch Division, Morton-Thiokol, Inc. (August 1, 1985).

71 Ritchie, R. O. and Horn, R. M., "Further Considerations on the Inconsistency in Toughness Evaluation of AISI 4340 Steel Austenitized at Increasing Temperatures", *Metallurgical Transactions*, Vol. 9A (March 1978), pp 331–341.

72 Gallagher, J., "Damage Tolerant Design Handbook", Metals and Ceramics Information Center, Battelle Columbus Division, Columbus, Ohio, MCIC-HB-01R (December 1983).

Fe
0.46 C
1.0 Cr
1.0 Mo
0.55 Ni

D6A
D6AC

Alloy	D6AC
AMS Specification	Product Form
6431F	Bars, Forgings, and Tubing, Premium Quality, Consumable Electrode Vacuum Melted
6438C	Sheet, Strip, Plate, Premium Aircraft Quality, Consumable Electrode Melted
5027B	Welding Wire, Vacuum Melted
5028A	Welding Wire, Vacuum Melted

TABLE 1.031. AMS SPECIFICATIONS (28, 29, 50, 51)

Alloy	D6AC					
AMS Specification	6431F, 6438C		5027B		5028A	
	Percent		Percent		Percent	
Element	Min	Max	Min	Max	Min	Max
Carbon	0.45	0.50	0.26	0.32	0.34	0.40
Chromium	0.90	1.20	0.90	1.20	0.90	1.20
Molybdenum	0.90	1.10	0.90	1.10	0.90	1.10
Nickel	0.40	0.70	0.40	0.70	0.40	0.70
Vanadium	0.08	0.15	0.05	0.10	0.05	0.10
Manganese	0.60	0.90	0.60	0.90	0.60	0.90
Silicon	0.15	0.30	0.10	0.30	0.15	0.30
Copper	–	0.35	–	0.35	–	0.35
Phosphorus	–	0.010(a)	–	0.010	–	0.008
Sulfur	–	0.010(a)	–	0.010	–	0.008
Oxygen	–	–	–	0.0025	–	0.0025
Nitrogen	–	–	–	0.0050	–	0.0050
Hydrogen	–	–	–	0.0010	–	0.0010

(a) 0.015 percent maximum for AMS 6438C.

TABLE 1.041. COMPOSITION (28, 29, 50, 51)

	Fe
0.46	C
1.0	Cr
1.0	Mo
0.55	Ni

D6A
D6AC

Alloy	D6AC			
	Procedures			
Form	Austenitize	Quench	Stress Relief(a)	Temper
Bars, Forgings, Tubing (28)	1650 – 1700 F, 40 min/in., 1 hr Min	Oil	390 – 410 F, 1 hr/in., 1 hr Min, AC	1025 – 1050 F, 2 hr/in., 4 hr Min
Sheet, Strip, Plate (29)	1600 – 1650 F ±10 F, 20 min Min	Oil	390 – 410 F, 1 hr, AC	≥1000 F, 4 hr Min, AC

(a) Snap temper.

TABLE 1.054. AMS CONVENTIONAL QUENCH AND TEMPER PROCEDURES

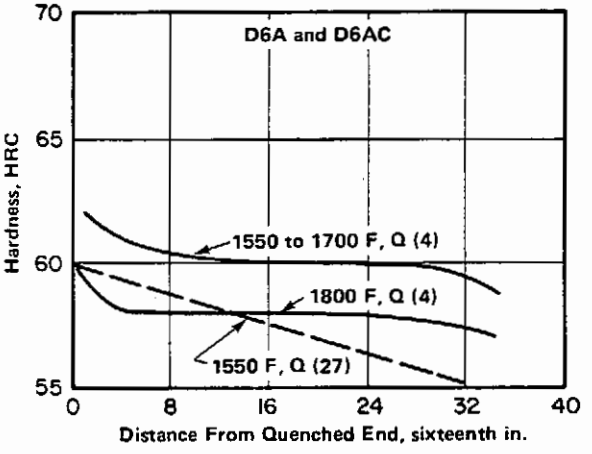

FIGURE 1.061. END QUENCH HARDENABILITY (4, 27)

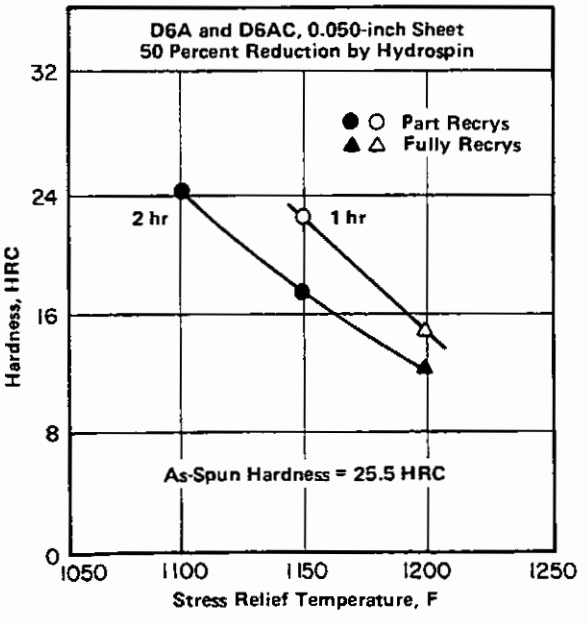

FIGURE 1.062. EFFECT OF STRESS RELIEF ON HARDNESS OF COLD WORKED SHEET (2)

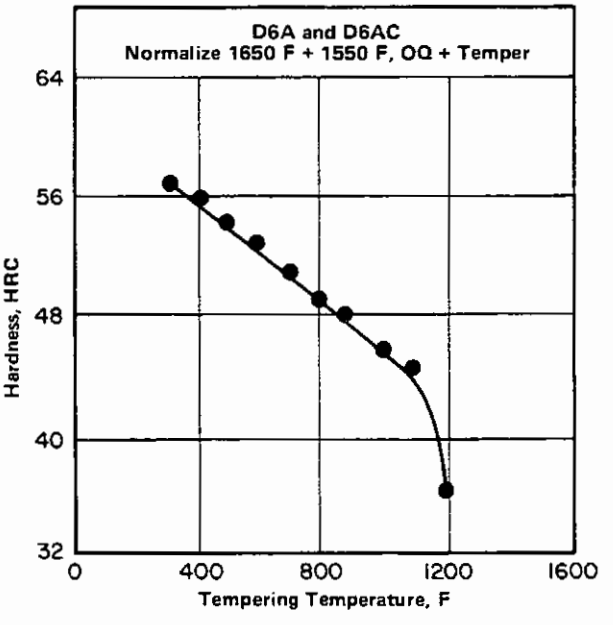

FIGURE 1.063. EFFECT OF TEMPERING TEMPERATURES ON HARDNESS (4)

	Fe
0.46	C
1.0	Cr
1.0	Mo
0.55	Ni

D6A
D6AC

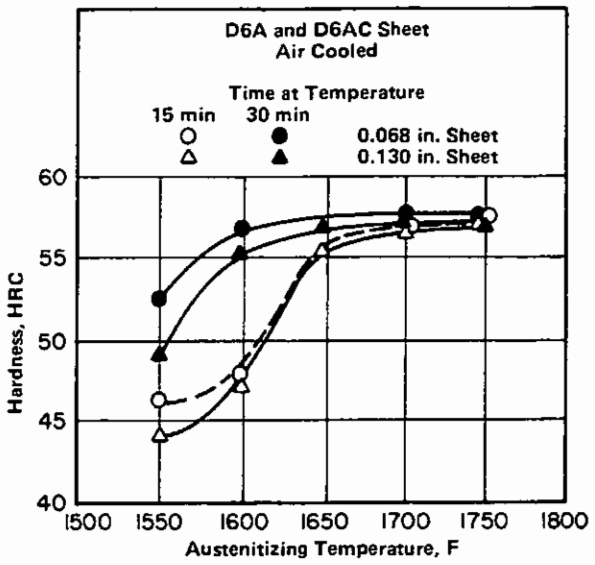

FIGURE 1.064. EFFECT OF AUSTENITIZING TEMPERATURE ON HARDNESS (43)

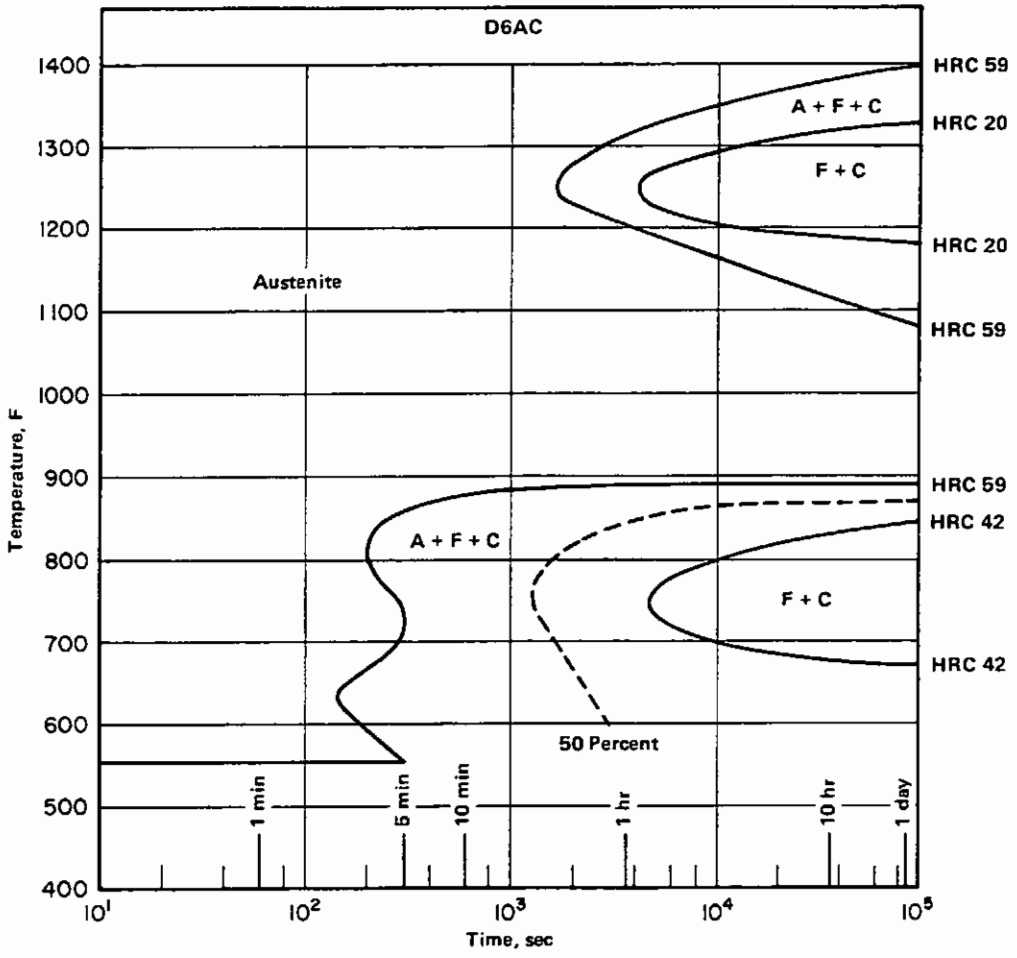

FIGURE 2.0121. TIME-TEMPERATURE-TRANSFORMATION DIAGRAM (53)

Fe
0.46 C
1.0 Cr
1.0 Mo
0.55 Ni

D6A
D6AC

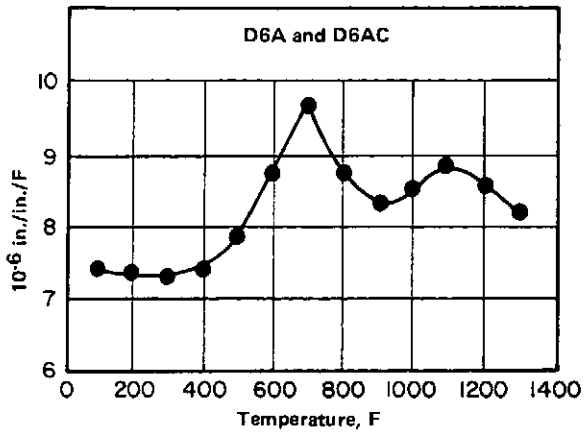

FIGURE 2.014. THERMAL EXPANSION

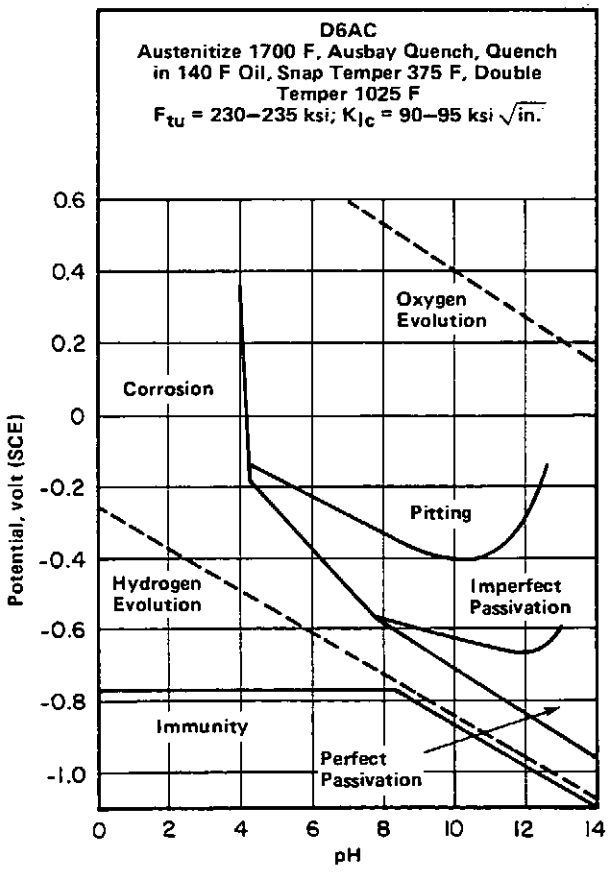

FIGURE 2.0312. POURBAIX DIAGRAM FOR CORROSION OF D6AC IN 0.1M NaCl (55)

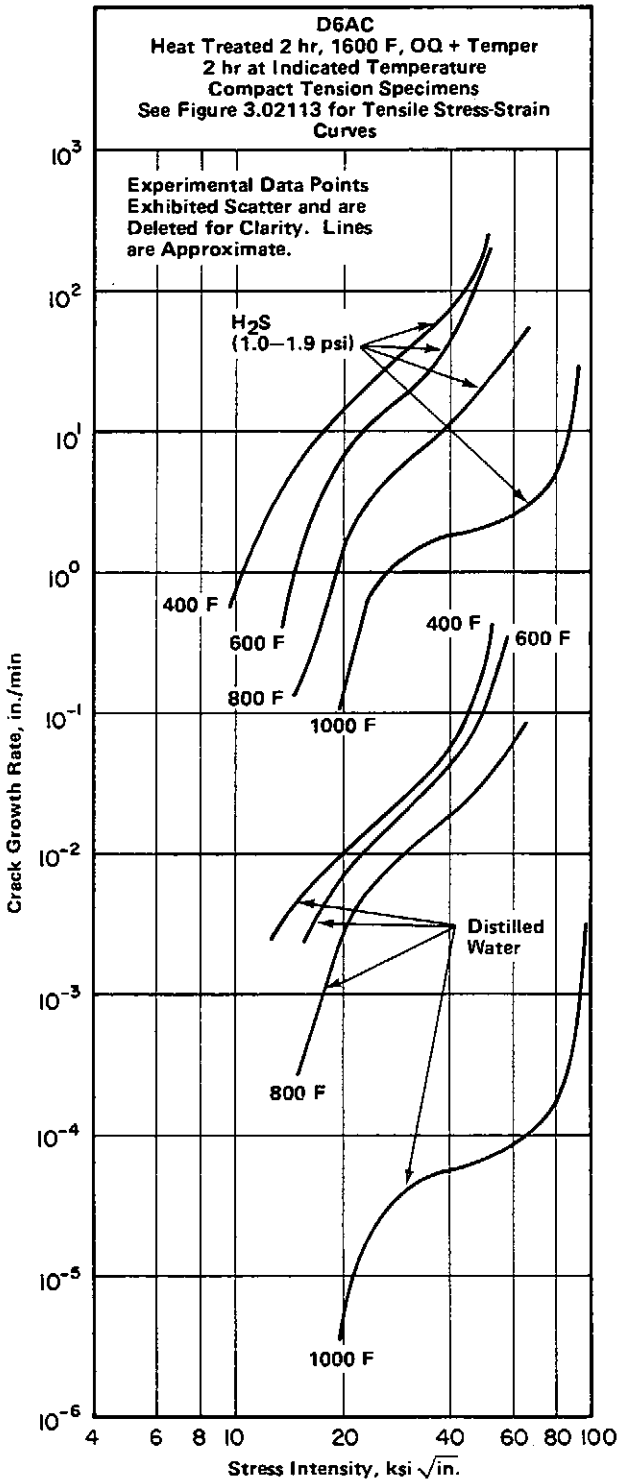

FIGURE 2.0322. EFFECTS OF TEMPERING TEMPERATURE ON STRESS-CORROSION CRACK-GROWTH BEHAVIOR IN WATER AND IN HYDROGEN SULFIDE (57)

	Fe
0.46	C
1.0	Cr
1.0	Mo
0.55	Ni

D6A
D6AC

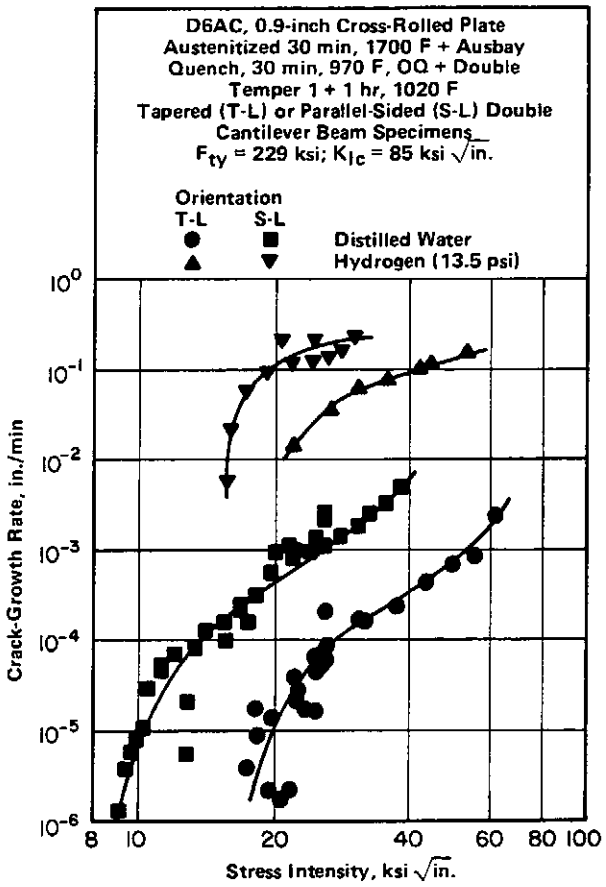

FIGURE 2.0324. EFFECTS OF ORIENTATION ON SUB-CRITICAL STRESS-CORROSION CRACK-GROWTH BEHAVIOR IN DISTILLED WATER AND IN HYDROGEN (58)

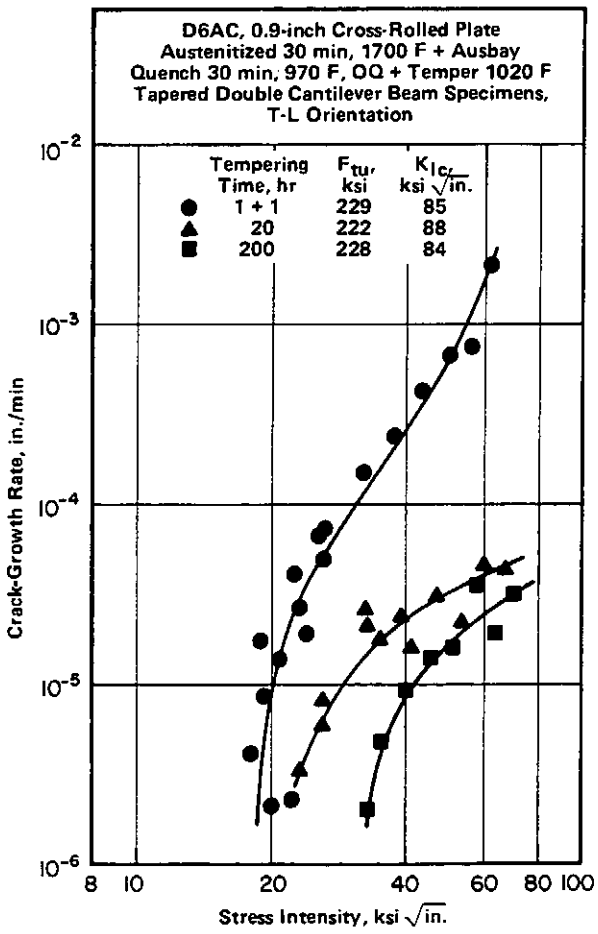

FIGURE 2.0325. EFFECT OF TEMPERING TIME AT 1020 F ON SUBCRITICAL STRESS-CORROSION CRACK-GROWTH BEHAVIOR IN DISTILLED WATER (58)

	Fe
0.46	C
1.0	Cr
1.0	Mo
0.55	Ni

D6A
D6AC

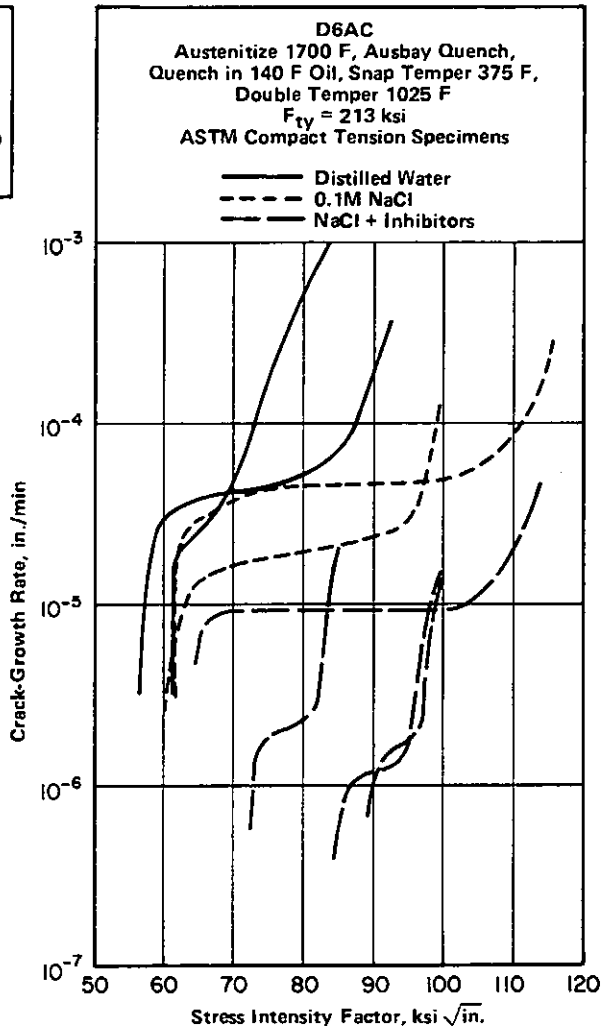

FIGURE 2.0327. EFFECTS OF INHIBITORS ON STRESS-CORROSION CRACK-GROWTH BEHAVIOR (60)

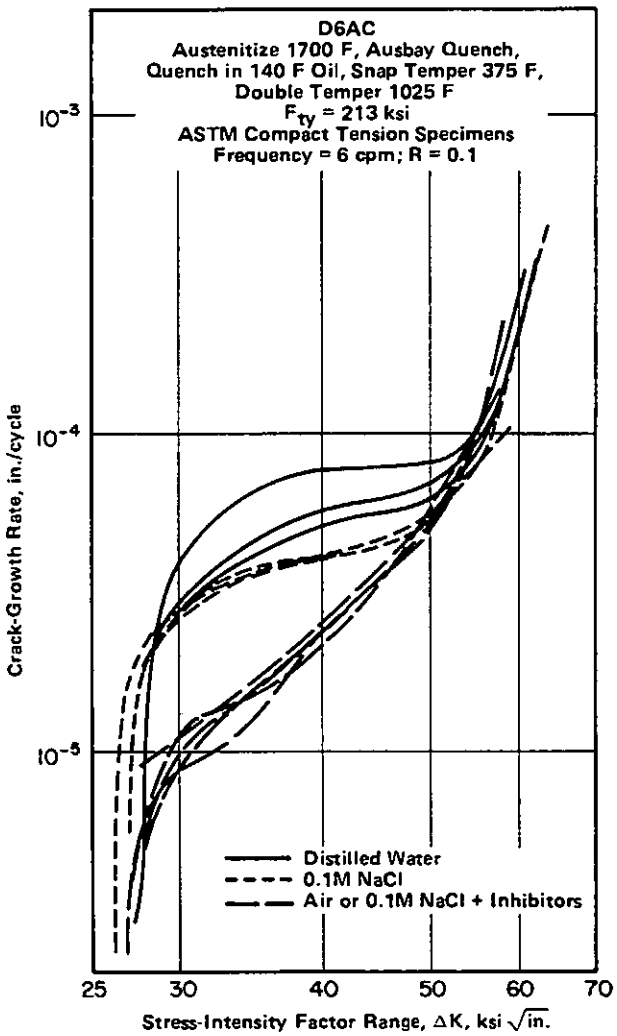

FIGURE 2.0328. EFFECTS OF INHIBITORS ON CORROSION FATIGUE CRACK-GROWTH BEHAVIOR (60)

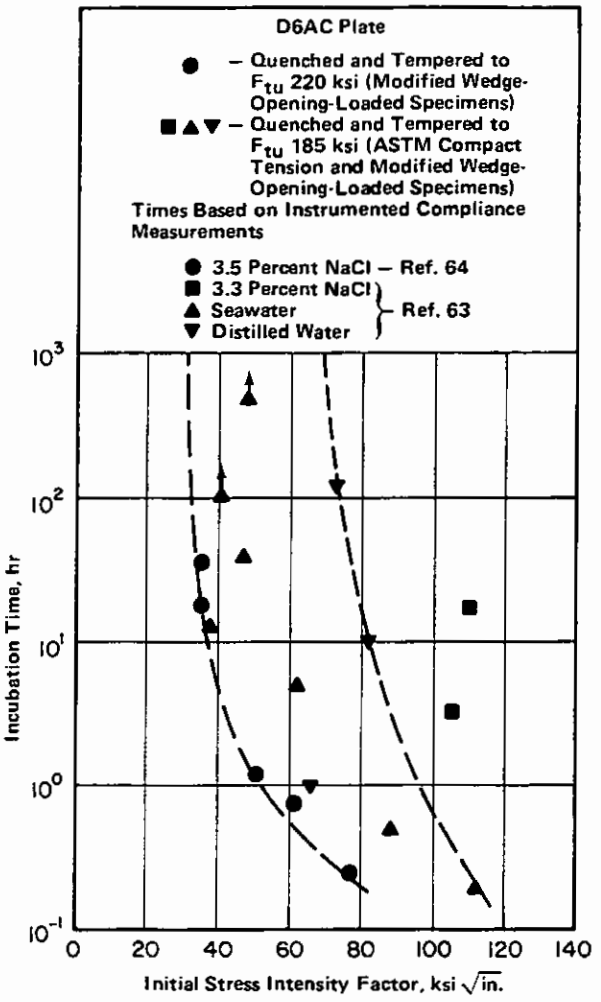

FIGURE 2.03211. INCUBATION TIMES FOR STRESS-CORROSION CRACK-GROWTH INITIATION IN AQUEOUS SOLUTIONS AS A FUNCTION OF INITIAL STRESS INTENSITY FACTOR (63, 64)

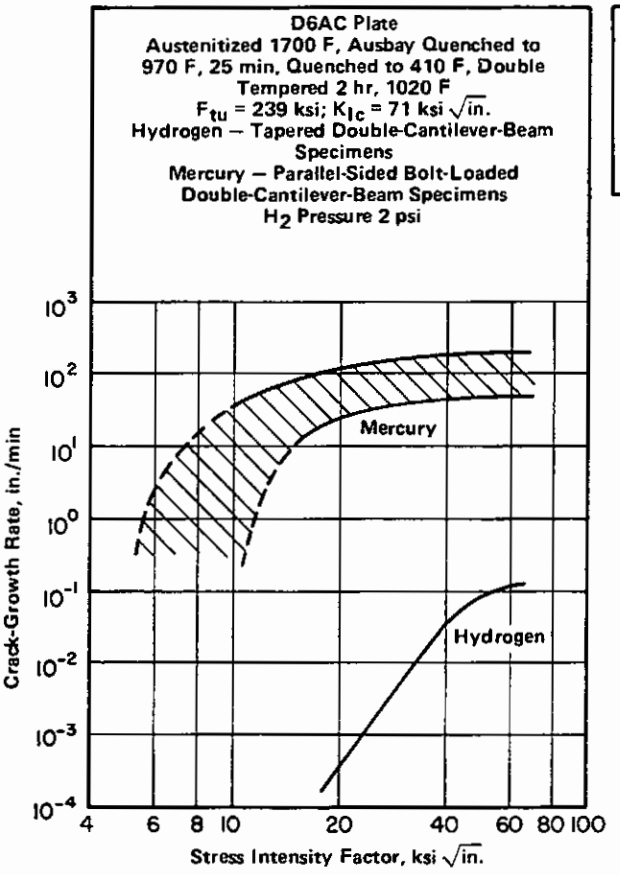

FIGURE 2.0331. STRESS-CORROSION CRACK-GROWTH BEHAVIOR IN LIQUID MERCURY AND LOW PRESSURE HYDROGEN ENVIRONMENTS (65)

Fe	
0.46	C
1.0	Cr
1.0	Mo
0.55	Ni

D6A
D6AC

Alloy	D6AC									
AMS Spec.	Product Form	Condition	Thickness, in.	F_{tu}, ksi Min	F_{tu}, ksi Max	F_{ty}, ksi Min	Elongation, %, Min	RA, %, Min	Hardness Min	Hardness Max
6431F	Bar	Cold Finished	≤0.500	–	145	–	–	–	–	–
		Hot Finished	>0.500	–	–	–	–	–	–	265 BHN
		Cold Finished	>0.500	–	–	–	–	–	–	285 BHN
	Mechanical Tubing	Cold Finished	–	–	–	–	–	–	–	25 HRC
		Hot Finished	–	–	–	–	–	–	–	285 BHN
	Bars, Forgings, Tubing	Heat Treated[a]	(Longitudinal)[b]	220	250	190	12	35	46 HRC	–
			(Transverse)[a]	220	250	190	9	30[d]	46 HRC	–
6438C	Sheet, Strip, Plate	Annealed or	–	–	–	–	–	–	–	–
		Norm. + Temp	–	–	–	–	–	–	–	30 HRC
		Spheroidize Ann.	–	–	–	–	–	–	–	100 HRB
		Heat Treated[a]	–	224	–	195	7	–	47 HRC[e]	–

Note: The original AMS document should be consulted for complete specification details.

(a) See Table 1.054 for heat treatment.
(b) Testing in longitudinal direction need not be performed on material tested in transverse direction.
(c) Tensile specimens must not be less than 2.50 in. in length.
(d) Average of all tests; any one test must be minimum of 25 percent reduction in area.
(e) Product shall not be rejected on basis of hardness if tensile properties are met.

TABLE 3.011. AMS SPECIFIED MECHANICAL PROPERTIES (28, 29)

	Fe
0.46	C
1.0	Cr
1.0	Mo
0.55	Ni

D6A
D6AC

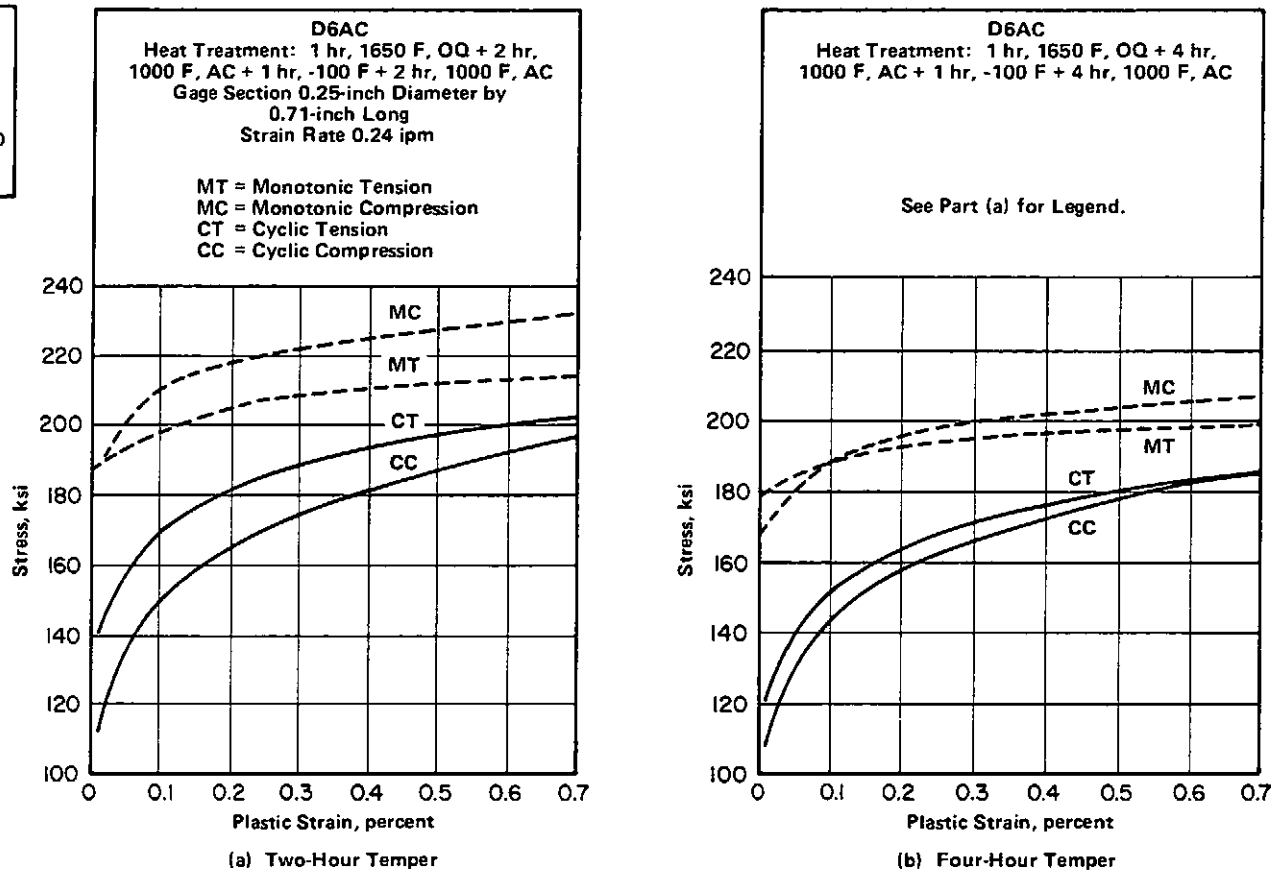

FIGURE 3.02112. MONOTONIC AND CYCLIC STRESS-STRAIN CURVES FOR TWO DIFFERENT HEAT TREATMENTS (52)

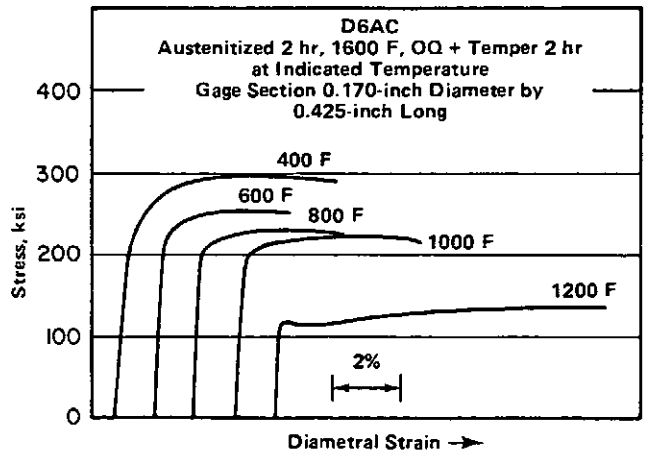

FIGURE 3.02113. EFFECTS OF TEMPERING TEMPERATURE ON STRESS-STRAIN CURVES AT ROOM TEMPERATURE (57)

	Fe
0.46	C
1.0	Cr
1.0	Mo
0.55	Ni

D6A
D6AC

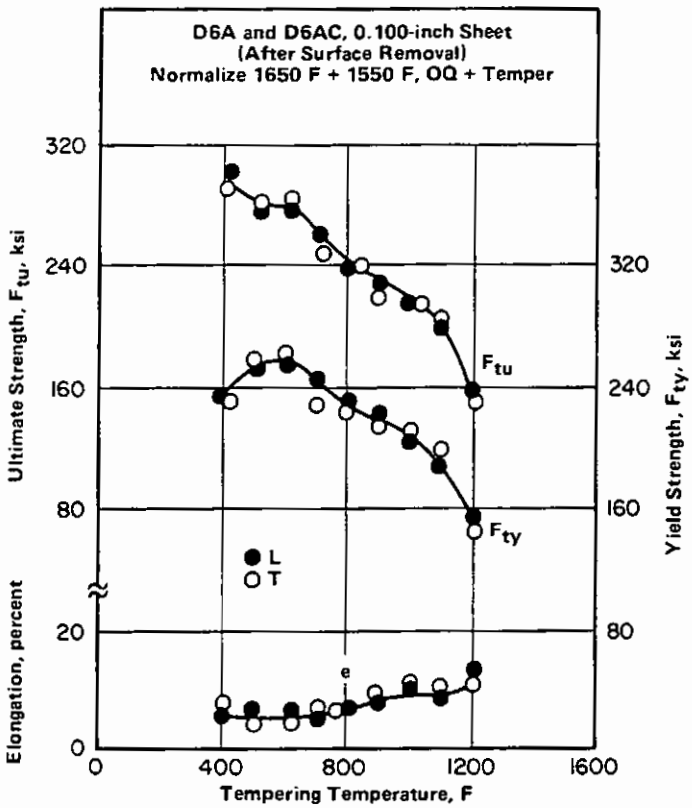

FIGURE 3.02121. EFFECT OF TEMPERING TEMPERATURE ON TENSILE PROPERTIES OF SHEET (4)

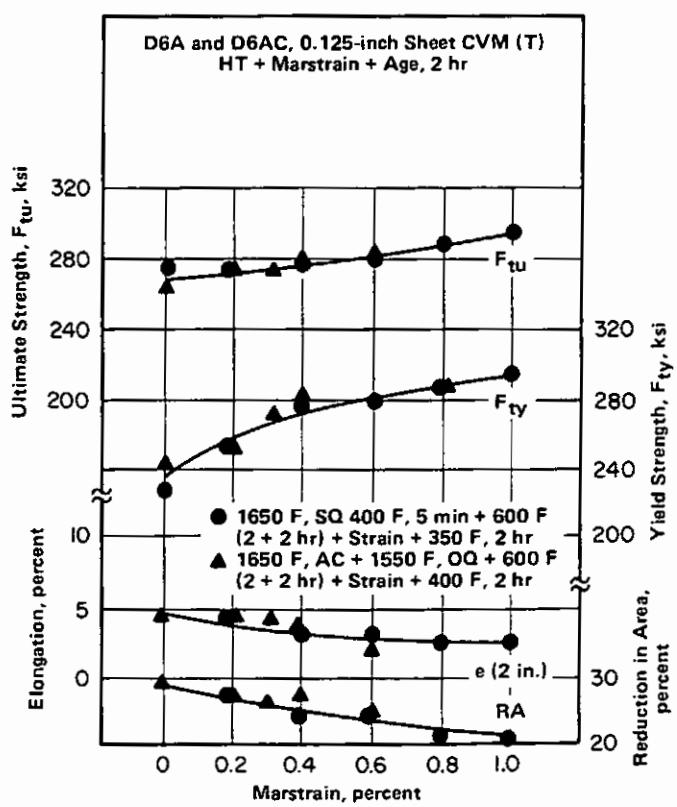

FIGURE 3.02122. EFFECT OF MARSTRAIN ON TENSILE PROPERTIES OF SHEET (11)

Fe	
0.46	C
1.0	Cr
1.0	Mo
0.55	Ni

D6A
D6AC

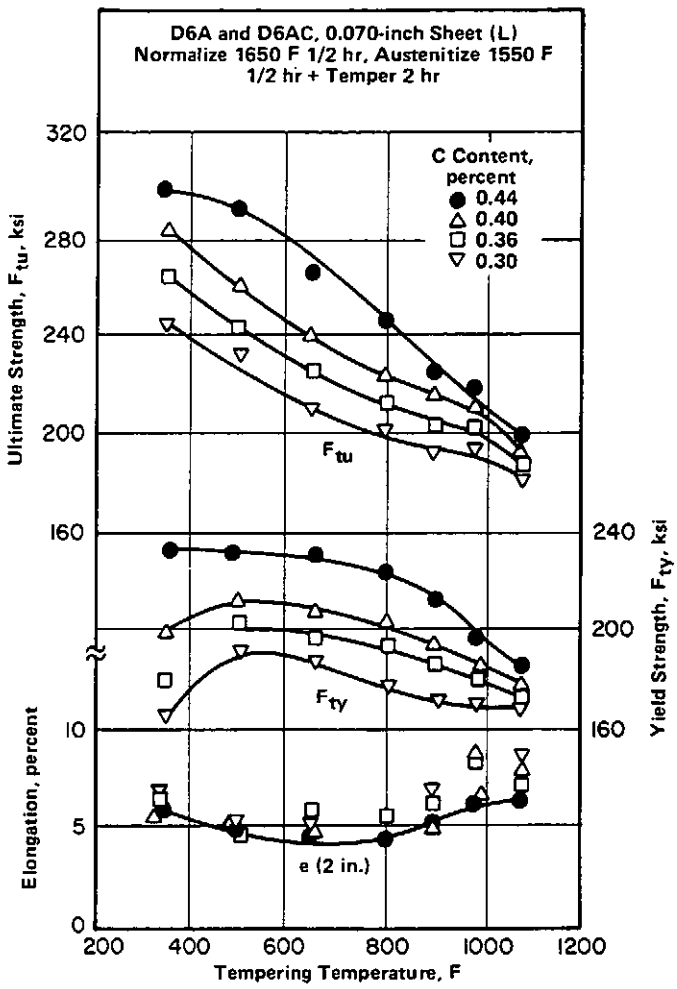

FIGURE 3.02123. EFFECT OF LOW CARBON CONTENT AND VARIOUS TEMPERING TEMPERATURES ON TENSILE PROPERTIES OF SHEET (31)

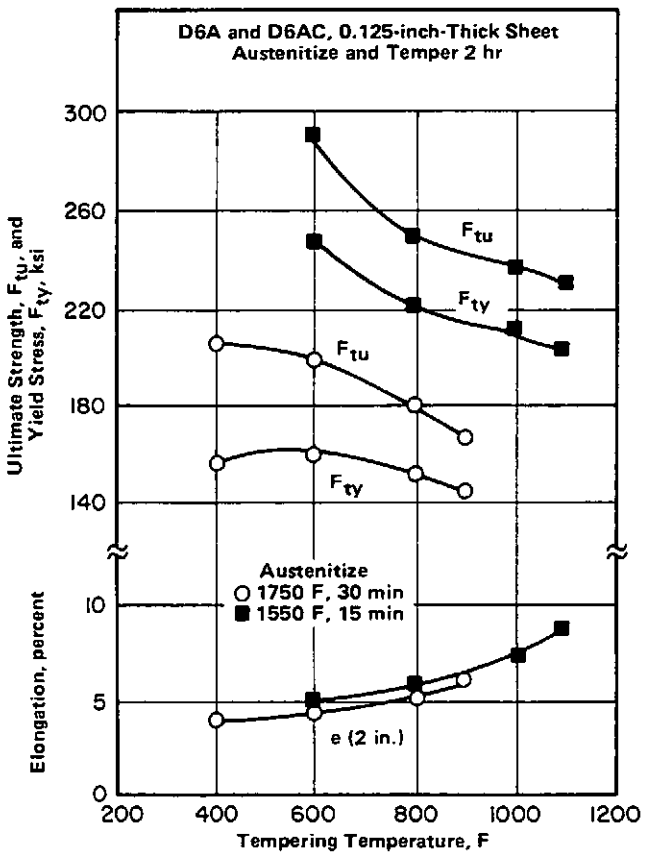

FIGURE 3.02124. EFFECT OF TEMPERING TEMPERATURE ON TENSILE PROPERTIES AT TWO AUSTENITIZING TEMPERATURES (41)

	Fe
0.46	C
1.0	Cr
1.0	Mo
0.55	Ni

D6A
D6AC

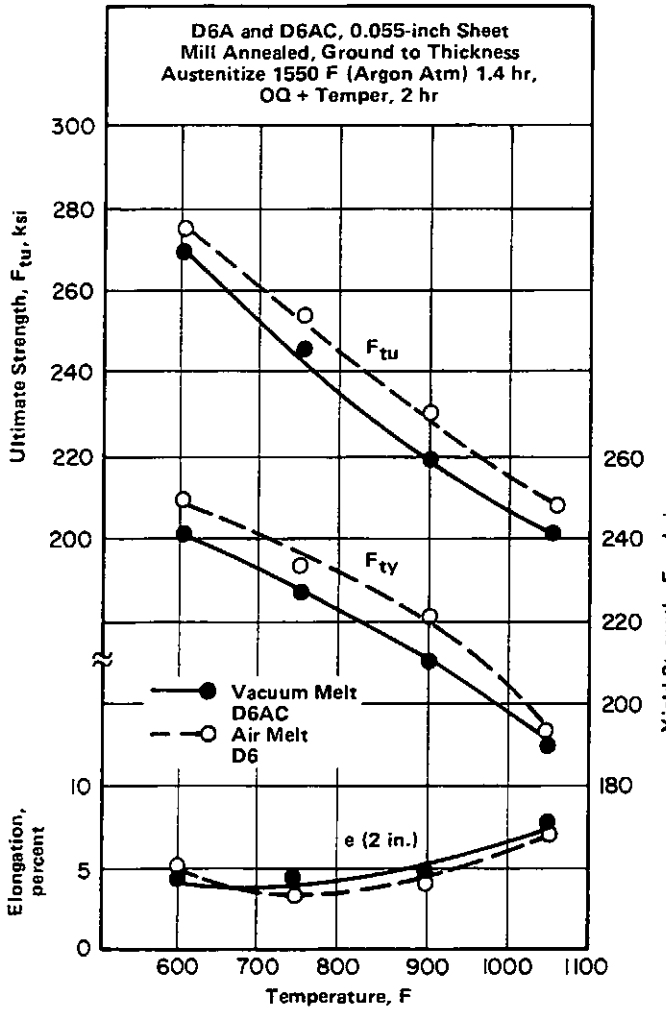

FIGURE 3.02125. EFFECT OF TEMPERING TEMPERATURE ON TENSILE PROPERTIES OF AIR AND VACUUM MELT ALLOY SHEET (36)

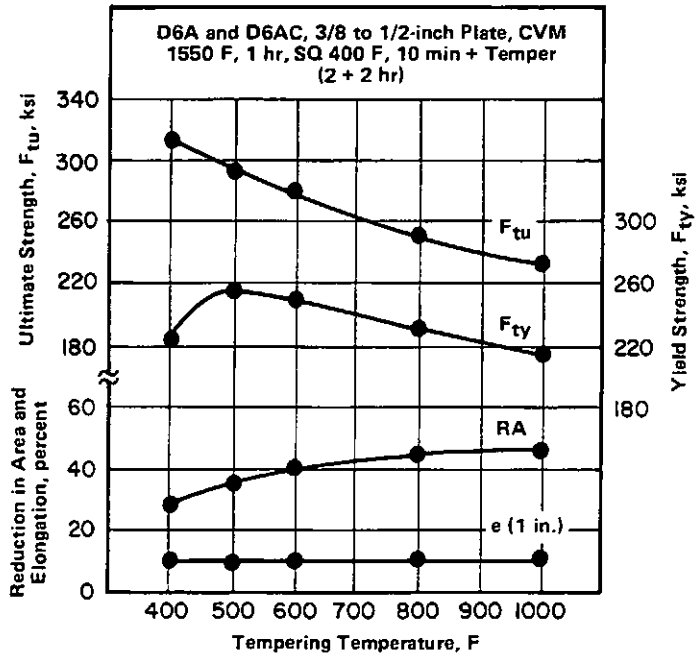

FIGURE 3.02131. EFFECT OF TEMPERING TEMPERATURE ON TENSILE PROPERTIES OF PLATE (18)

Alloy	D6A – D6AC
Form	Plate
Condition	1650 F, 1 hr OQ (140 F) + 500 to 550 F Temper
F_{tu}, ksi	275
Range	268 – 284
F_{ty}, ksi	233
Range	225 – 245

TABLE 3.02132. RANGE OF TENSILE PROPERTIES IN PLATES TEMPERED AT 500 TO 550 F (49)

	Fe
0.46	C
1.0	Cr
1.0	Mo
0.55	Ni

D6A
D6AC

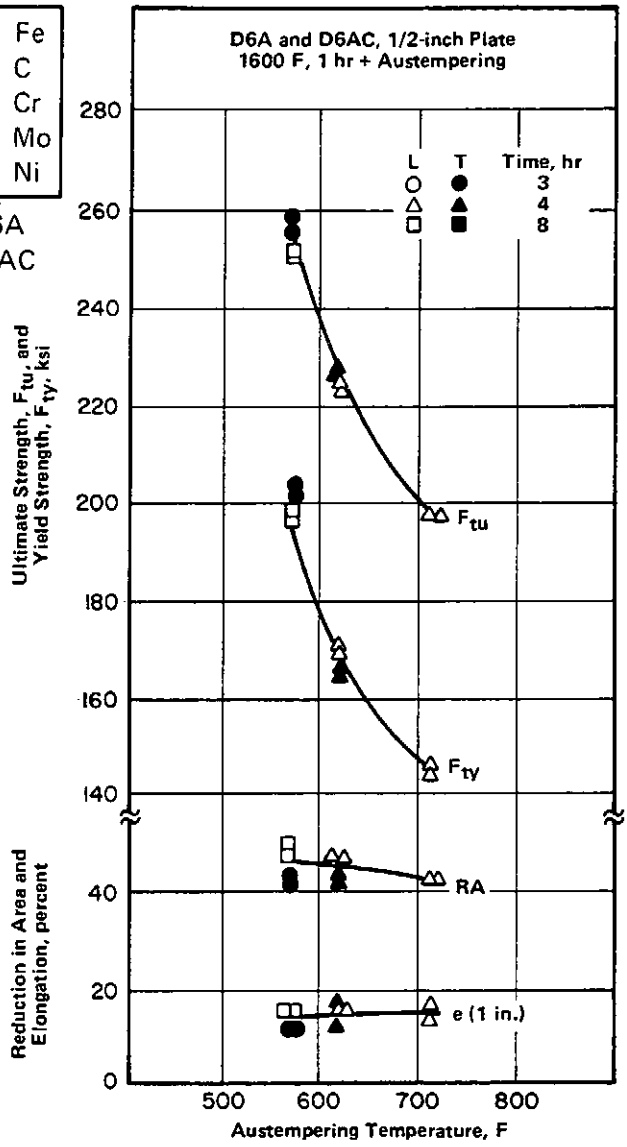

FIGURE 3.02133. EFFECT OF AUSTEMPERING TEMPERATURE ON TENSILE PROPERTIES OF PLATE (39)

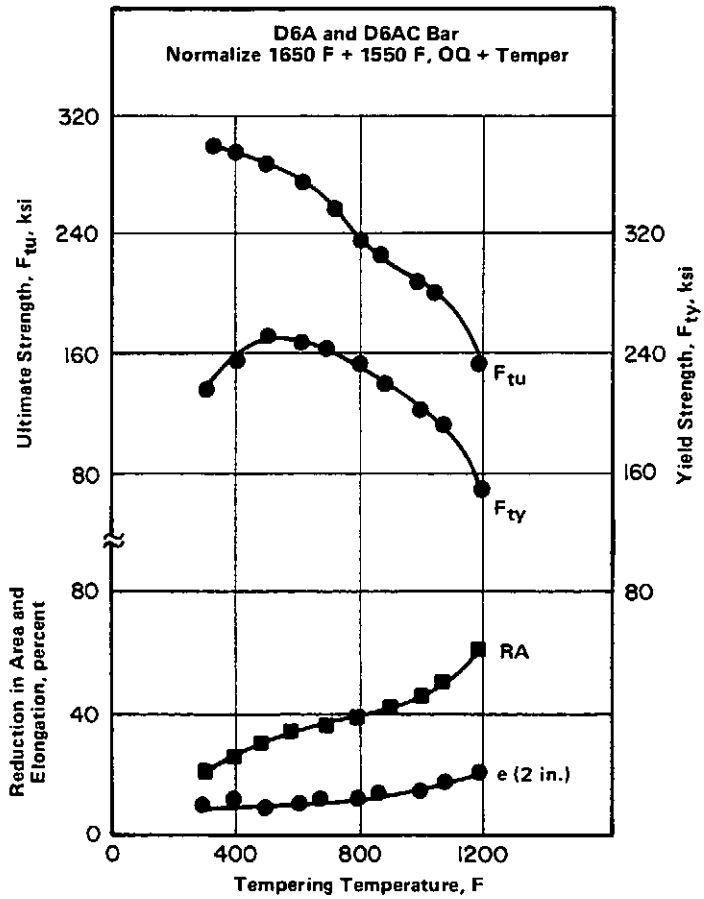

FIGURE 3.02141. EFFECT OF TEMPERING TEMPERATURE ON TENSILE PROPERTIES OF BAR (4)

	Fe
0.46	C
1.0	Cr
1.0	Mo
0.55	Ni

D6A
D6AC

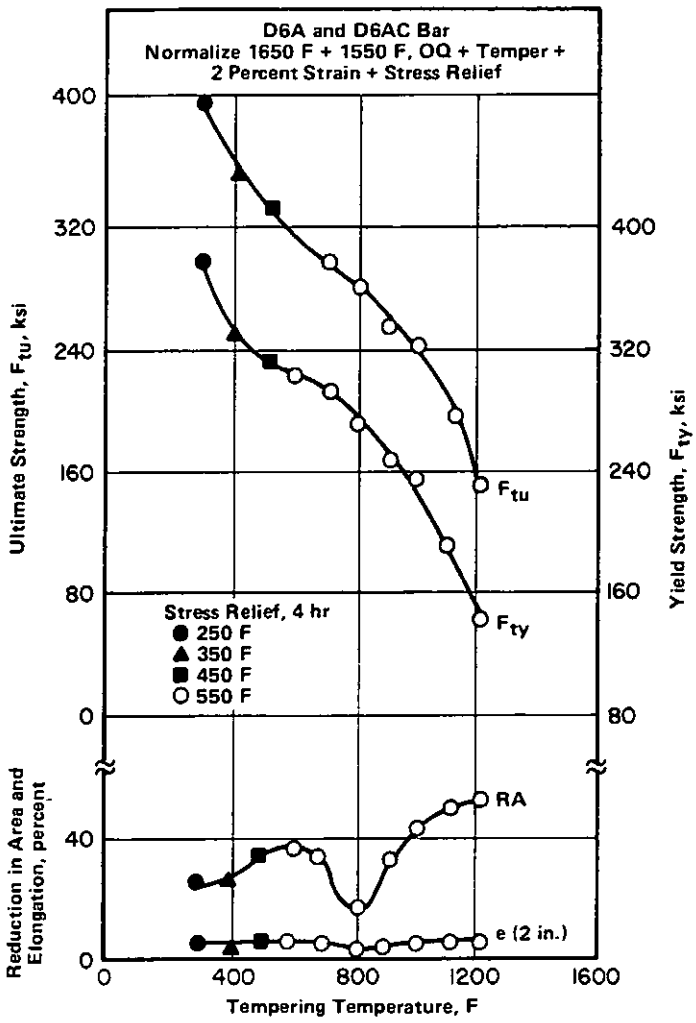

FIGURE 3.02142. EFFECT OF TEMPERING TEMPERATURE ON TENSILE PROPERTIES OF STRAIN-AGED BAR (4)

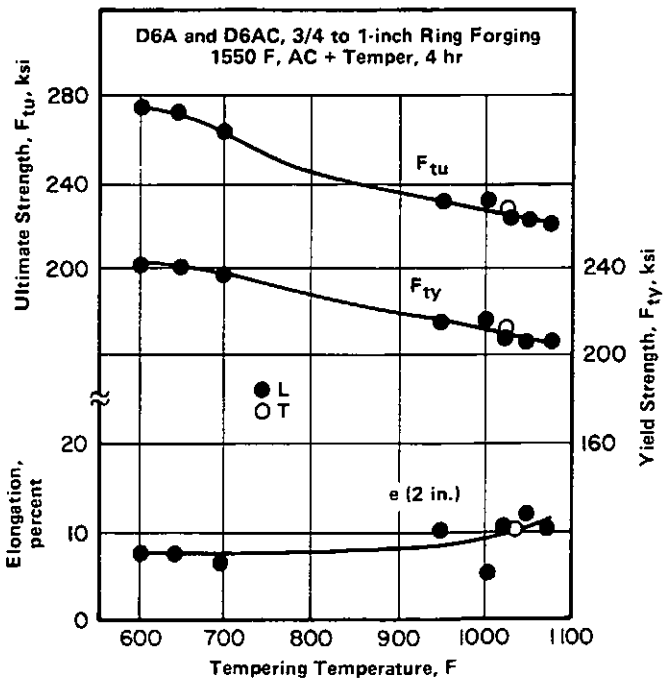

FIGURE 3.02151. EFFECT OF TEMPERING TEMPERATURE ON TENSILE PROPERTIES OF ROLLED RING FORGINGS (13)

	Fe
0.46	C
1.0	Cr
1.0	Mo
0.55	Ni

D6A
D6AC

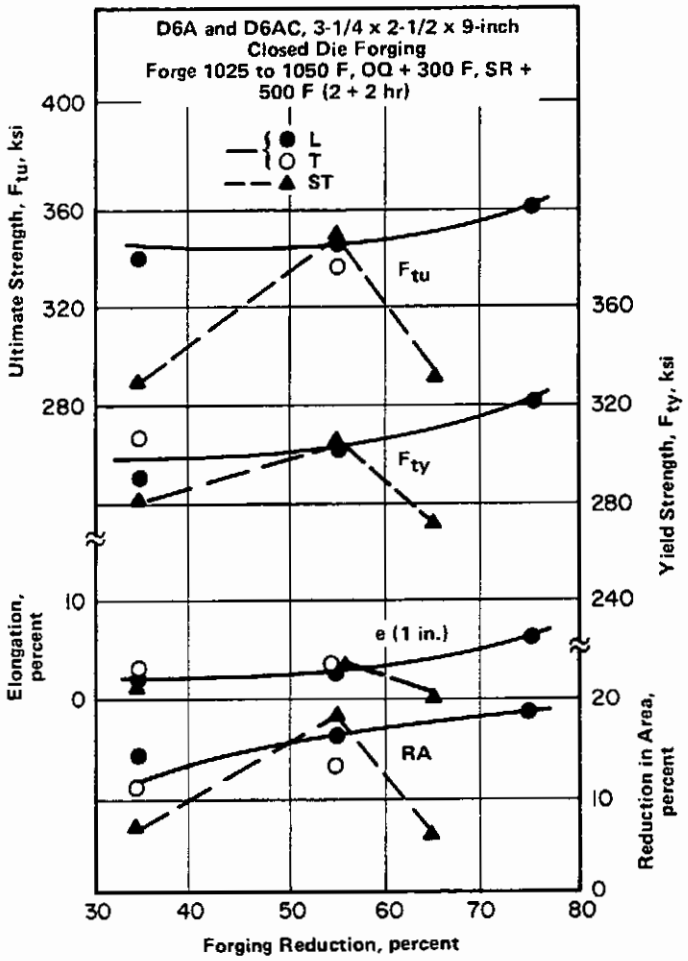

FIGURE 3.02152. EFFECT OF FORGING REDUCTION ON TENSILE PROPERTIES OF A VARIABLE-CROSS-SECTION AUSFORMED FORGING TEMPERED AT 500 F (10)

	Fe
0.46	C
1.0	Cr
1.0	Mo
0.55	Ni

D6A
D6AC

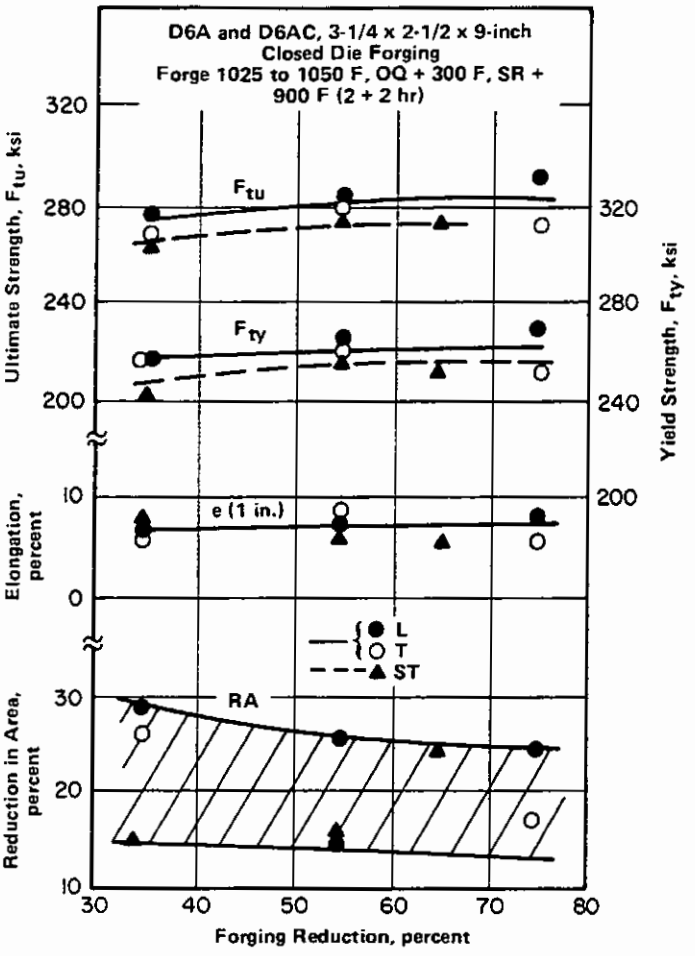

FIGURE 3.02153. EFFECT OF FORGING REDUCTION ON TENSILE PROPERTIES OF A VARIABLE-CROSS-SECTION AUSFORMED FORGING TEMPERED AT 900 F (10)

	Fe
0.46	C
1.0	Cr
1.0	Mo
0.55	Ni

D6A
D6AC

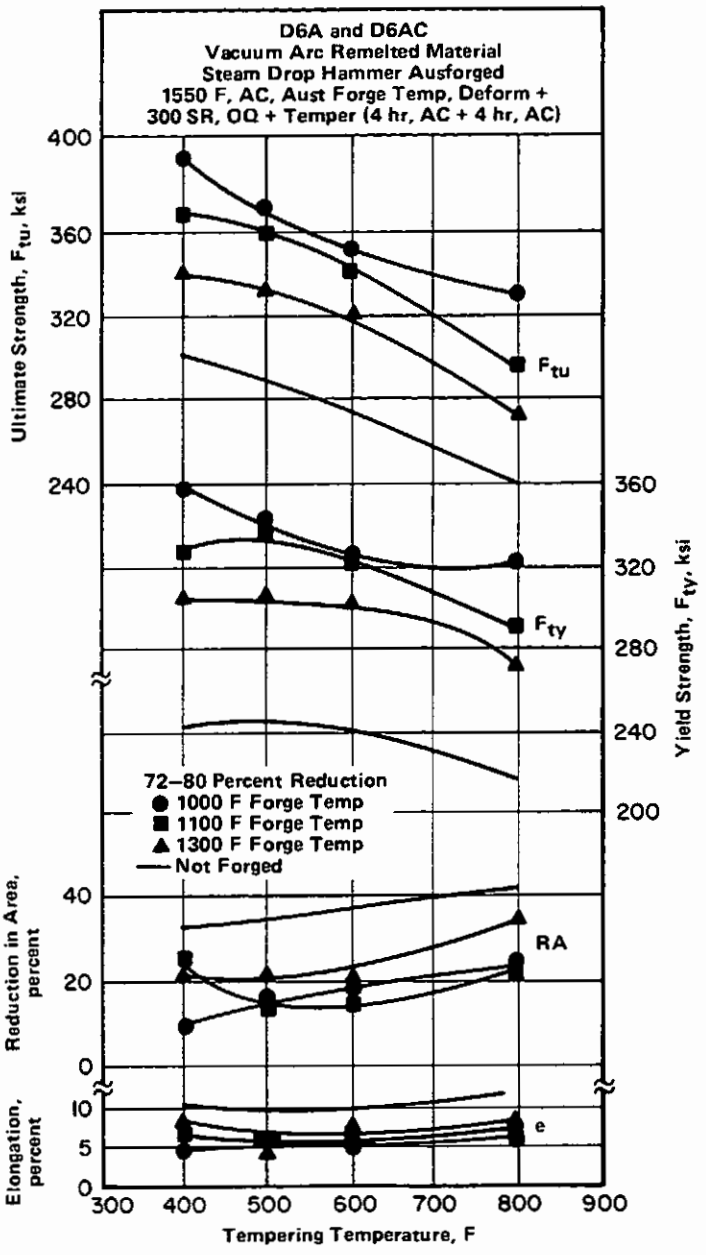

FIGURE 3.02154. EFFECT OF FORGING AND TEMPERING TEMPERATURE ON TENSILE PROPERTIES OF AUSFORMED FORGINGS (32)

	Fe
0.46	C
1.0	Cr
1.0	Mo
0.55	Ni

D6A
D6AC

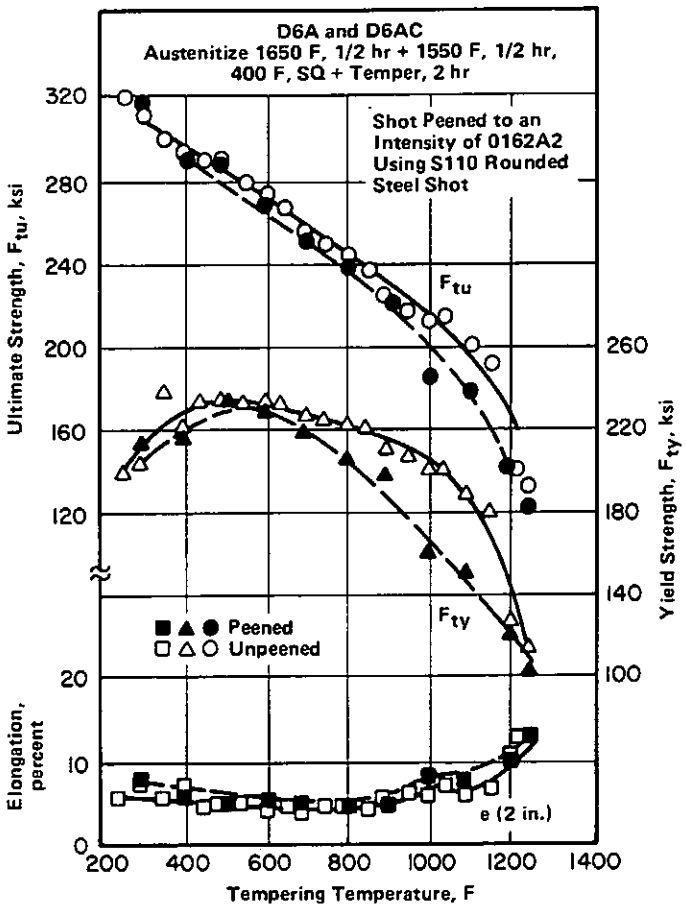

FIGURE 3.02155. EFFECT OF SHOT PEENING AND TEMPERING TEMPERATURE ON TENSILE PROPERTIES (35)

	Fe
0.46	C
1.0	Cr
1.0	Mo
0.55	Ni

D6A
D6AC

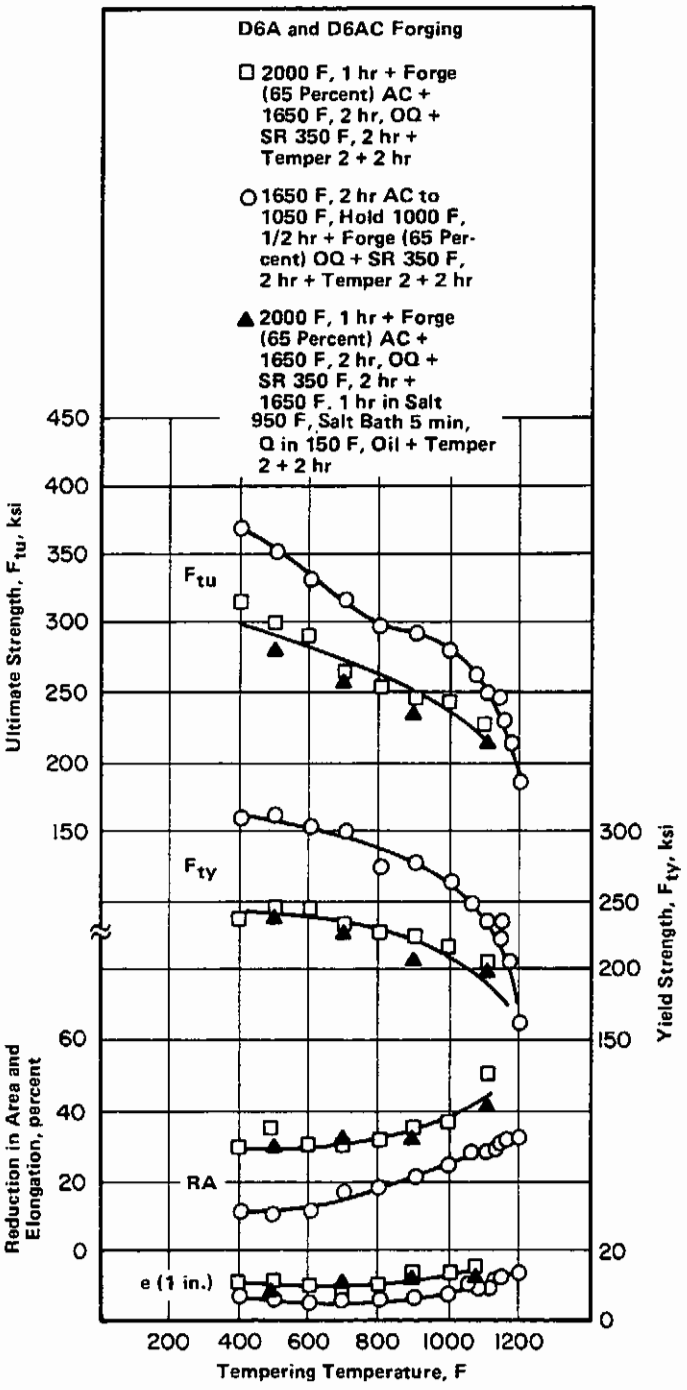

FIGURE 3.02156. EFFECT OF TEMPERING TEMPERATURE ON TENSILE PROPERTIES FOR THREE THERMAL-MECHANICAL PROCESSING TREATMENTS OF FORGED ALLOY (42)

Alloy	D6A – D6AC									
Form	T-Shaped Extrusion 4-3/4 x 4-3/8 x 72 in. (CVM) With 3/8 and 5/8 in.-Thick Legs									
Condition	1650 F, 30 min, FC + 1625 F, 30 min, 950 F, 1 hr, 400 F Salt, 15 min, AC + Temper (2 + 2 hr)									
Temper	650 F					1025 F				
Location	Center	5/8 in. Leg		3/8 in. Leg		Center	5/8 in. Leg		3/8 in. Leg	
Direction	L	L	T	L	T	L	L	T	L	T
F_{tu}, ksi	290	285	281	282	284	239	238	236	239	237
F_{ty}, ksi	255	248	254	245	250	218	218	218	220	219
e (1 in.), percent	12	11	9	12	10	15	13	12	13	12
RA, percent	40	38	34	42	35	49	30	40	52	42

	Fe
0.46	C
1.0	Cr
1.0	Mo
0.55	Ni

D6A
D6AC

TABLE 3.02161. TENSILE PROPERTIES OF EXTRUSION AT TWO TEMPERING TEMPERATURES (14)

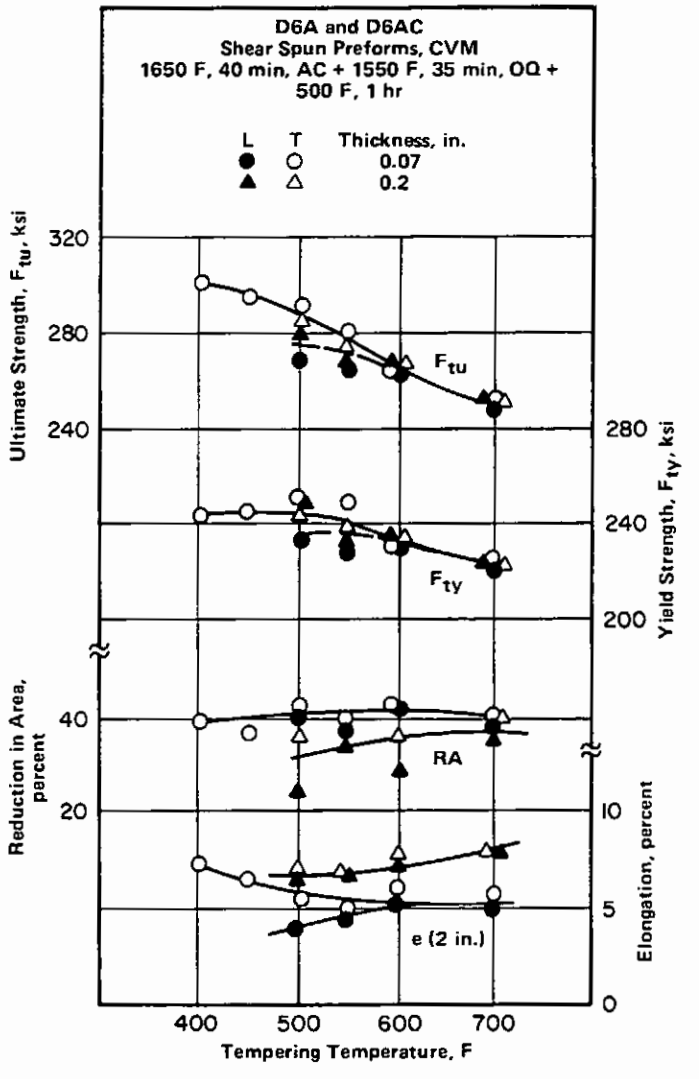

FIGURE 3.02171. EFFECT OF TEMPERING TEMPERATURE ON TENSILE PROPERTIES OF SHEAR SPUN ALLOY (19)

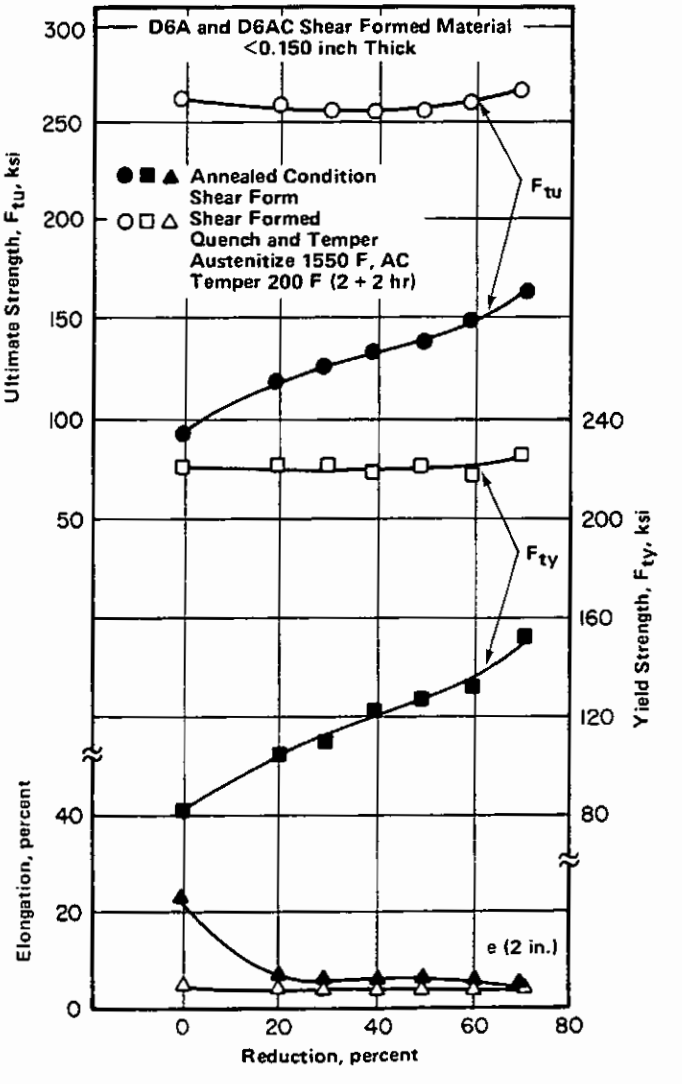

FIGURE 3.02172. EFFECT OF SHEAR FORM REDUCTION ON TENSILE PROPERTIES (33)

	Fe
0.46	C
1.0	Cr
1.0	Mo
0.55	Ni

D6A
D6AC

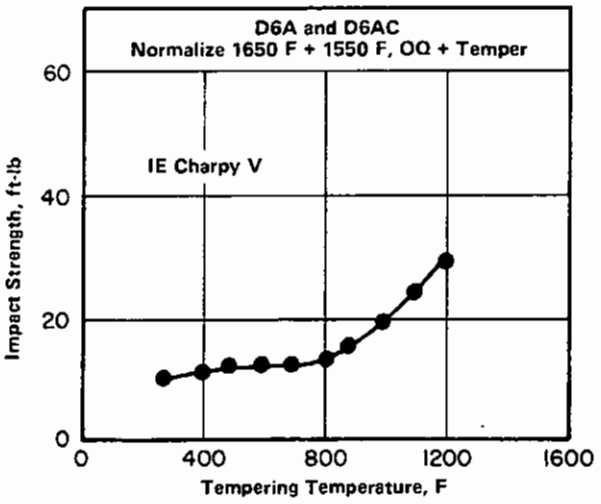

FIGURE 3.0231. EFFECT OF TEMPERING TEMPERATURE ON IMPACT PROPERTIES (4)

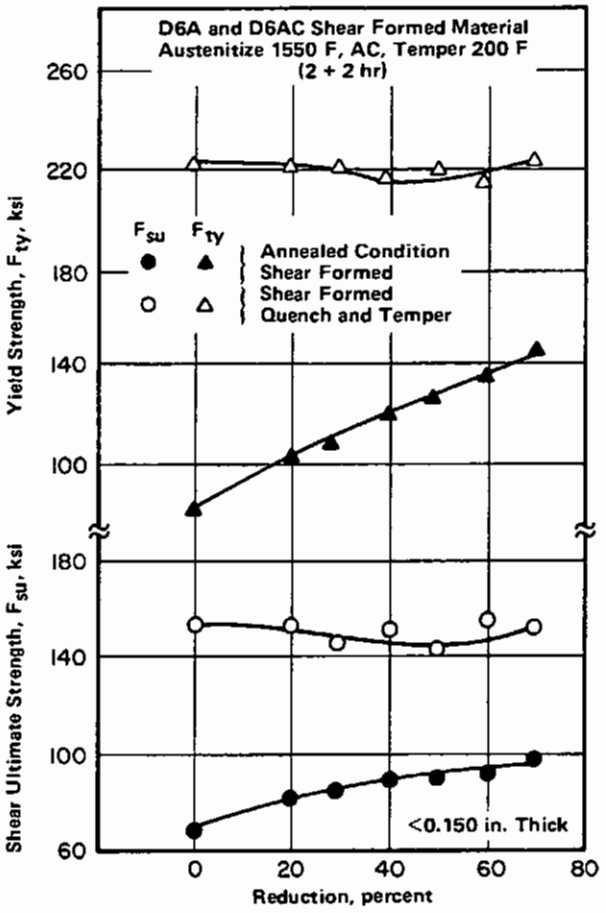

FIGURE 3.0251. EFFECT OF SHEAR FORM REDUCTION ON SHEAR STRENGTH (33)

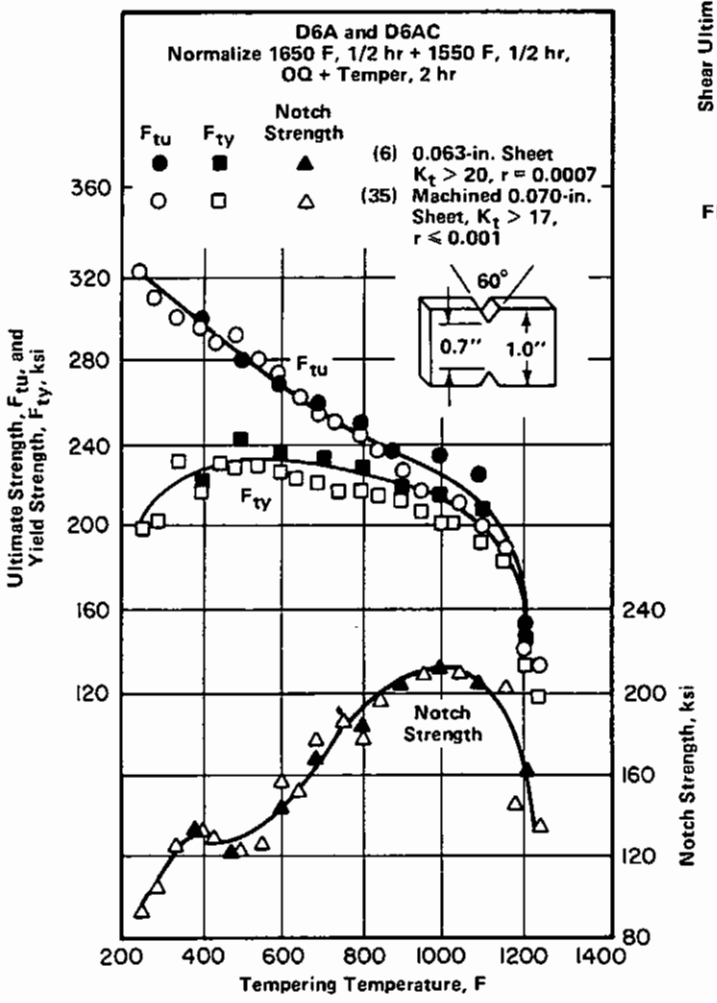

FIGURE 3.027111. EFFECT OF TEMPERING TEMPERATURE ON SHARP NOTCH PROPERTIES OF SHEET (6, 35)

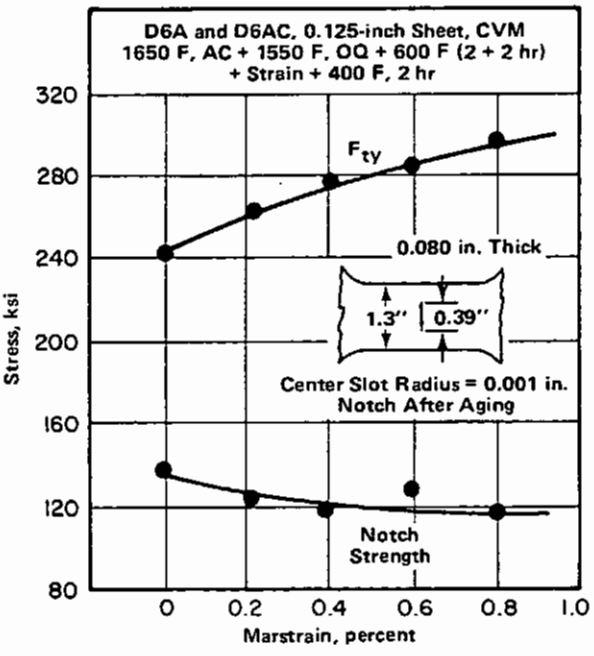

FIGURE 3.027112. EFFECT OF MARSTRAIN ON SHARP NOTCH PROPERTIES OF SHEET (11)

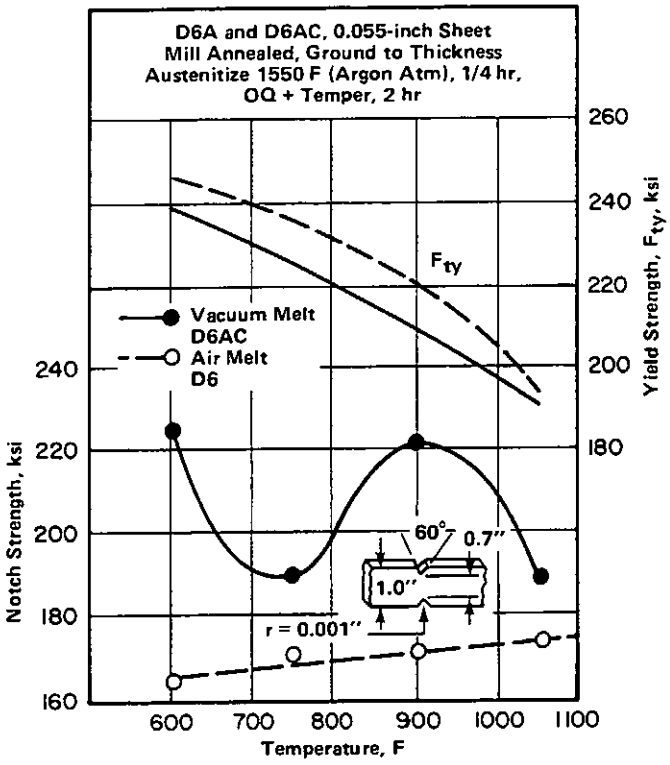

FIGURE 3.027113. EFFECT OF TEMPERING TEMPERATURE ON SHARP NOTCH PROPERTIES OF AIR AND VACUUM MELT SHEET (36)

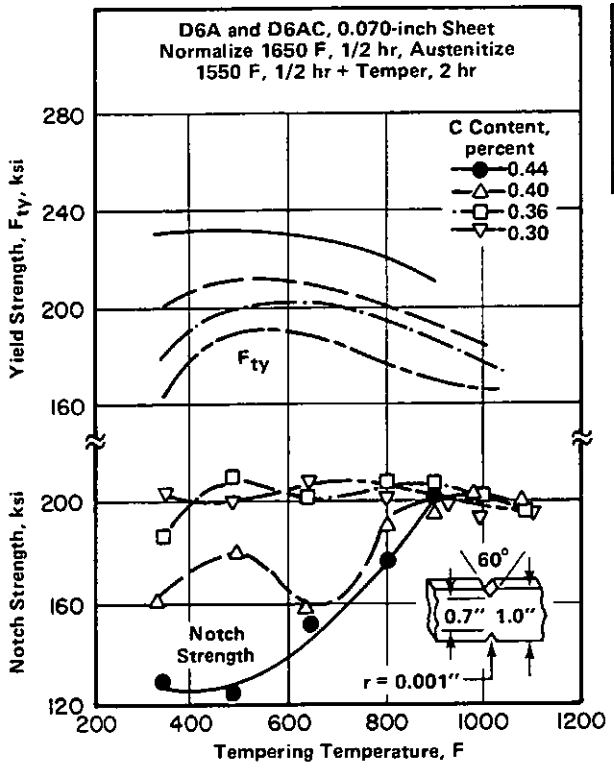

	Fe
0.46	C
1.0	Cr
1.0	Mo
0.55	Ni

D6A
D6AC

FIGURE 3.027114. EFFECT OF LOW CARBON CONTENT AND TEMPERING TEMPERATURE ON SHARP NOTCH STRENGTH OF SHEET (31)

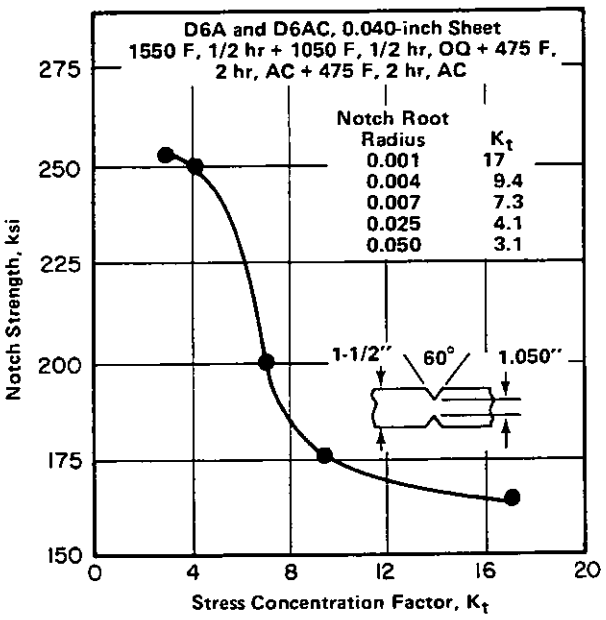

FIGURE 3.027115. EFFECT OF NOTCH ROOT RADII ON SHARP NOTCH STRENGTH OF SHEET (34)

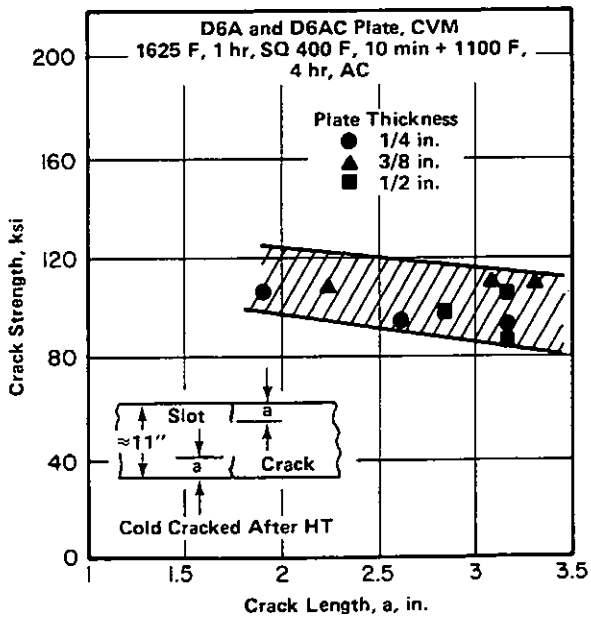

FIGURE 3.027121. EFFECT OF CRACK LENGTH ON CRACK STRENGTH OF THREE THICKNESSES OF PLATE EACH FROM DIFFERENT HEAT (24)

	Fe
0.46	C
1.0	Cr
1.0	Mo
0.55	Ni

D6A
D6AC

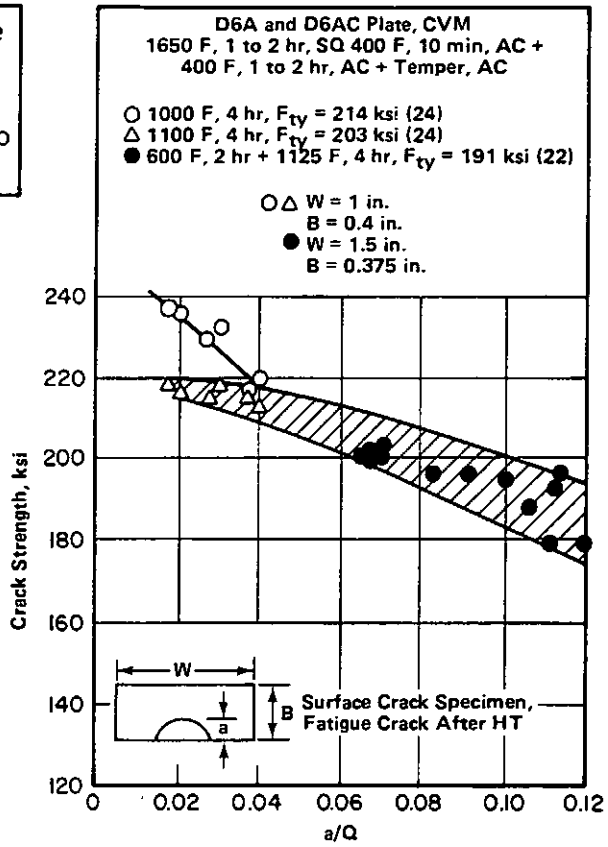

FIGURE 3.027122. EFFECT OF SURFACE CRACKS ON CRACK STRENGTH OF PLATE AT STRENGTH LEVELS BETWEEN F_{ty} = 190 AND 215 KSI (22, 24)

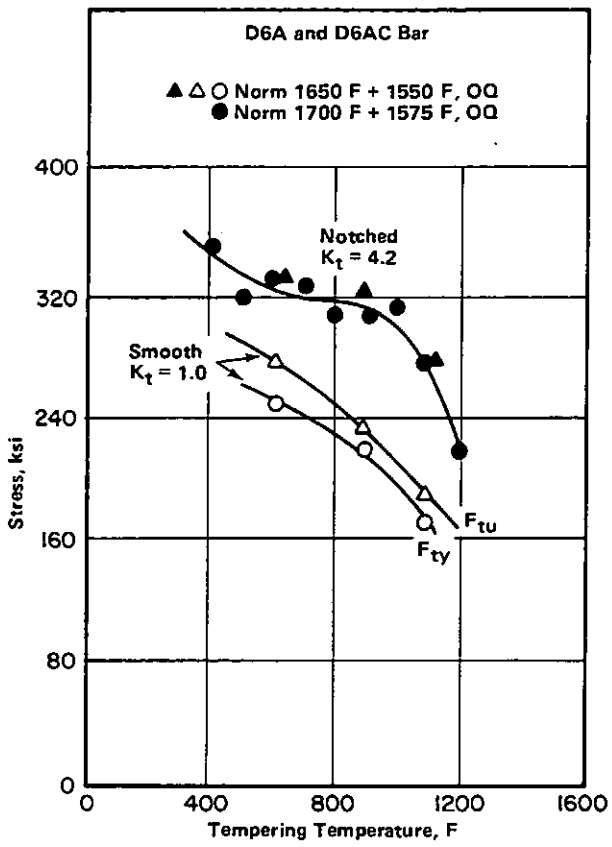

FIGURE 3.027131. EFFECT OF TEMPERING TEMPERATURE ON NOTCH AND SMOOTH TENSILE PROPERTIES OF BAR (4)

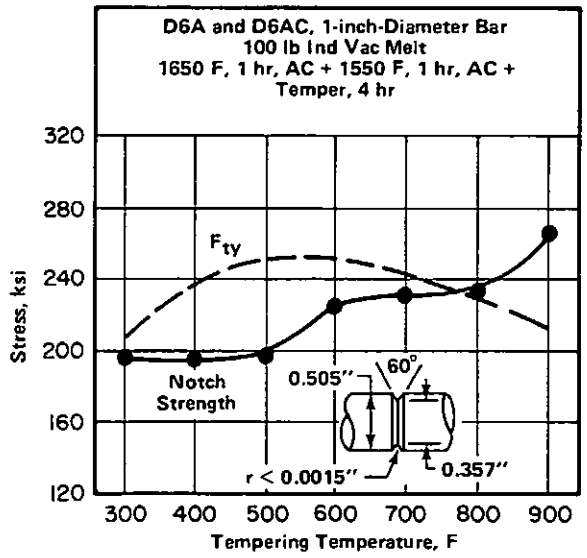

FIGURE 3.027132. EFFECT OF TEMPERING TEMPERATURE ON THE SHARP NOTCH STRENGTH OF BAR (16)

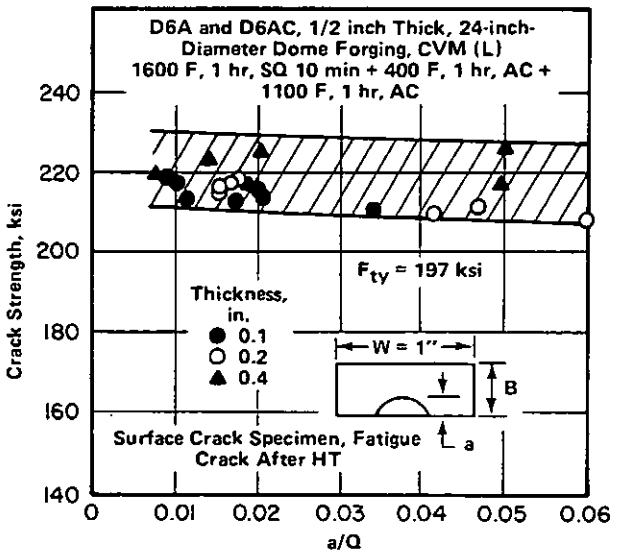

FIGURE 3.027141. EFFECT OF SURFACE CRACKS ON CRACK STRENGTH OF FORGING (23)

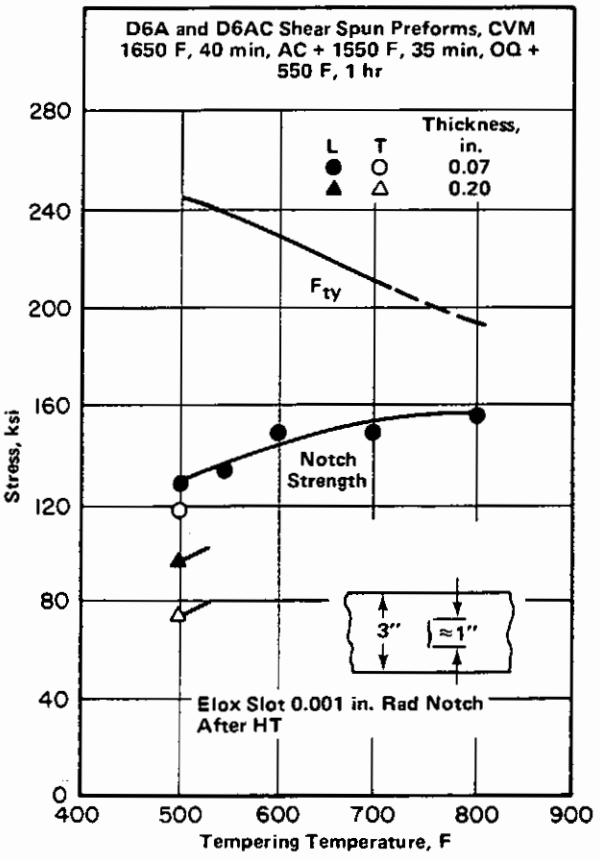

FIGURE 3.02715. EFFECT OF TEMPERING TEMPERATURE ON SHARP NOTCH PROPERTIES OF SHEAR SPUN ALLOY (19)

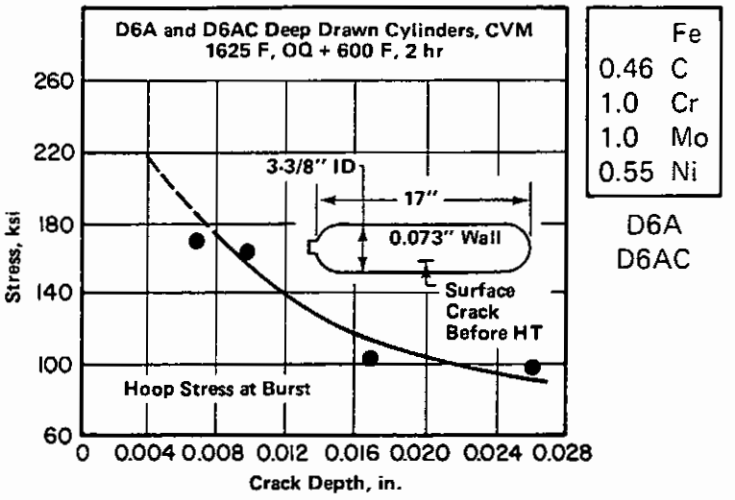

FIGURE 3.02716. EFFECT OF SURFACE CRACKS ON BURST STRENGTH OF THIN WALLED CYLINDERS (15)

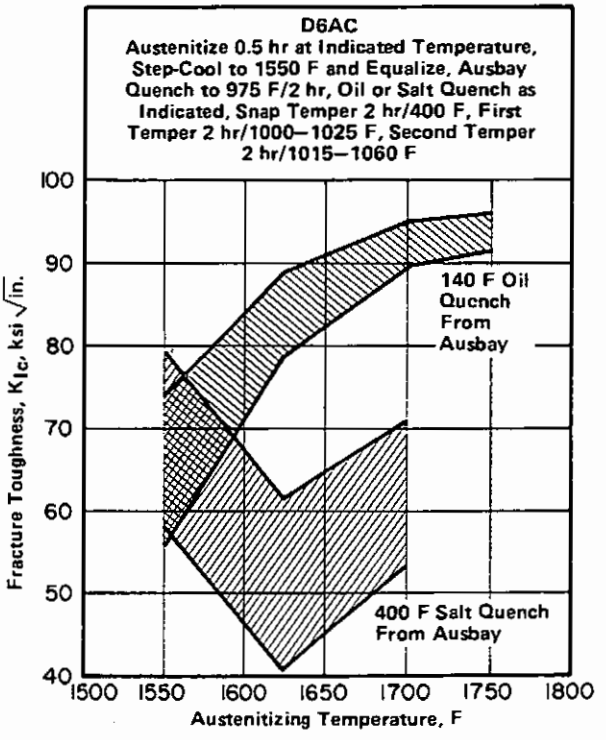

FIGURE 3.02722. EFFECTS OF AUSTENITIZING TEMPERATURE AND QUENCH MEDIUM ON FRACTURE TOUGHNESS (53)

	Fe
0.46	C
1.0	Cr
1.0	Mo
0.55	Ni

D6A
D6AC

Alloy	D6A – D6AC	
Form	0.8-in. Plate (CVM), LT (for F_{ty} see Table 3.0314)	
Condition	A	E (Slack Quench)
K_{Ic}, ksi $\sqrt{in.}$	95(a)	64(b)
Range	(83 – 102)	(44 – 91)

(a) Average of 21.
(b) Average of 82.
Condition A: 1700 F + Ausbay quench to 975 F in furnace + quench in 140 F oil + temper at 1000 F to 1025 F, 2 + 2 hr + AC.
Condition E: 1650 F + Ausbay quench to 975 F in furnace + quench in 400 F salt + temper at 1000 F to 1025 F, 2 + 2 hr + AC.

TABLE 3.02723. PLANE STRAIN FRACTURE TOUGHNESS OF 0.8-INCH-THICK CVM PLATE (45)

Alloy	D6A – D6AC	
Form	0.8 and 1.5 – 1.8 in. Forging (CVM), LT (for F_{ty} see Table 3.0315)	
Condition	A & B	E (Slack Quench)
K_{Ic}, ksi $\sqrt{in.}$	95(a)	65(b)
Range	(85 – 109)	(47 – 96)

(a) Average of 34.
(b) Average of 60.
Conditions A & B: 1700 F + Ausbay quench to 975 F in furnace + quench in 140 F oil + temper at 1000 F to 1025 F, 2 + 2 hr + AC.
Condition E: 1650 F + Ausbay quench to 975 F in furnace + quench in 400 F salt + temper at 1000 F to 1025 F, 2 + 2 hr + AC.

TABLE 3.02724. PLANE STRAIN FRACTURE TOUGHNESS OF CVM FORGINGS (45)

Alloy	D6A – D6AC	
Condition	1650 F 1 hr, OQ (140 F) + 500 – 550 F Temper	
Form	Plate	Forging (Complex Part)
Thickness	≤2 in.	≈1-1/2 in.
Slack Quench	No	Yes
F_{ty}, ksi	233	233
K_{Ic}, ksi $\sqrt{in.}$	56	52
Range	(54 – 59)	(35 – 59)

TABLE 3.02725. PLANE STRAIN FRACTURE TOUGHNESS OF PLATE AND FORGED PARTS (49)

Fe
0.46 C
1.0 Cr
1.0 Mo
0.55 Ni

D6A
D6AC

Alloy	D6AC								
Heat Treatment Temperature, F				Mechanical Properties					
					Fracture Toughness				
Austenitize	Ausbay	Quench	Temper	F_{ty}, ksi	Specimen Thickness, in.	Specimen Orientation	K_{Ic}, ksi $\sqrt{in.}$	Std. Dev., ksi $\sqrt{in.}$	No. Tests
Plate									
Heat Treated to HRC 46				206	0.70	T-L	85.8	1.8	2
1675/AC + 1575	None	OQ	2H/400 + 2H/1100	–	1.0	–	77.2	1.0	4
1675/AC + 1575	None	OQ	2H/400 + 2H/1100	–	1.0	–	53.7	1.6	4
1675/AC + 1575	None	OQ	2H/400 + 2H/500	–	1.0	–	34.5	1.2	4
Forgings									
2.25H/1615	None	325	3H/310–345 + 6–6.5/1080	199	1.0	L-S	64.7	5.5	3
	Same HT			201	1.0	T-L	78.4	15.1	6
	Same HT			187–203	1.0	S-L	83.9	14.8	52
1650	960	OQ, 180	2+2H/1025	219	0.50	–	87.7	0.7	3
Billets									
1H/1650/FC + 1H/1650	None	OQ	2+2H/1025	210	1.0	L-T	78.5	4.7	2
1H/1650	960	OQ, 150	2+2H/1000	211	1.0	L-T	80.3	0.8	2
1700	960	OQ, 150	2+2H/1000	215	1.0	L-T	80.3	4.3	3
1700	None	OQ	2+2H/1025	214–216	1.0	L-T	77.3	2.4	6
1H/1725/AC + 1H/1700	None	OQ	1H/1000 + 1H/1025	213	1.0	L-T	77.2	2.7	3
1H/1725/AC + 1H/1700	None	OQ	2+2H/1100	200–205	1.0	L-T	101.2	6.1	5
1H/1725/AC + 1H/1700	None	OQ	2+2H/1025	213–217	1.0	L-T	74.4	6.2	6
1H/1725/AC +1H/1650	960	SQ, 350	2+2H/1025	221	1.0	L-T	75.1	10.1	3

TABLE 3.02726. EFFECTS OF HEAT TREATMENT ON FRACTURE TOUGHNESS OF PLATE, FORGINGS, AND BILLETS AT ROOM TEMPERATURE (72)

D6AC, 1-inch Diameter Bar, Specimen Quench Size = 0.75-inch-Thick Blocks							
Heat Treatment Temperature, F				Mechanical Properties			
Austenitize	Ausbay	Quench	Temper	F_{ty}, ksi	F_{tu}, ksi	K_{Ic}, ksi $\sqrt{in.}$(a)	Std. Dev., ksi $\sqrt{in.}$
1700	970	OQ, 140	1025	211	233	94.2	2.7
1700	970	OQ, 140	1050	208	230	95.4	–
1700	970	OQ, 140	1075	205	229	100.6	1.8
1700	970	OQ, 140	618	217	259	54.6	1.5
1700	970	OQ, 140	550	219	278	45.0	1.0
1700	None	OQ, 140	1025	211	235	95.5	3.1
1700	970	SQ, 410	1025	210	235	77.7	2.0
1700	970	SQ, 365	1025	211	235	88.0	2.2
1700	970	AC	1025	210	239	42.2	3.3
1650	970	AC	1025	207	229	34.8	1.8

(a) Average of 2 to 6 values. Fracture toughness was measured on standard ASTM E399/72T compact tension specimens.

TABLE 3.02727. EFFECTS OF HEAT TREATMENT ON FRACTURE TOUGHNESS OF BAR (66)

Fe	
0.46	C
1.0	Cr
1.0	Mo
0.55	Ni

D6A
D6AC

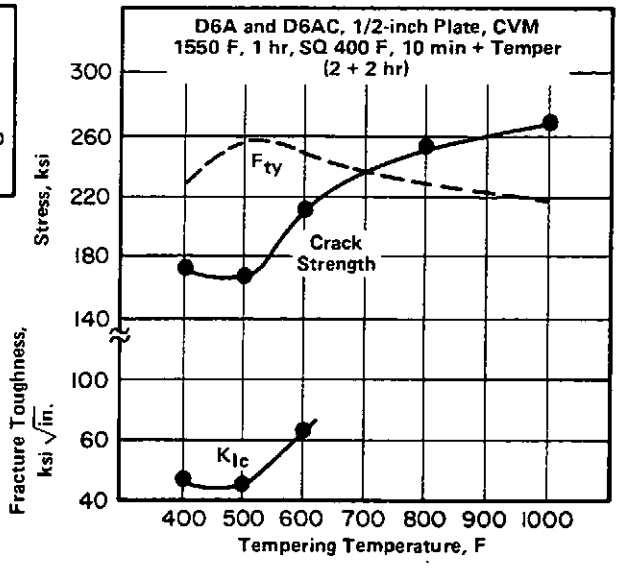

FIGURE 3.02729. EFFECT OF TEMPERING TEMPERATURE ON SHARP NOTCH PROPERTIES AND FRACTURE TOUGHNESS OF PLATE (18)

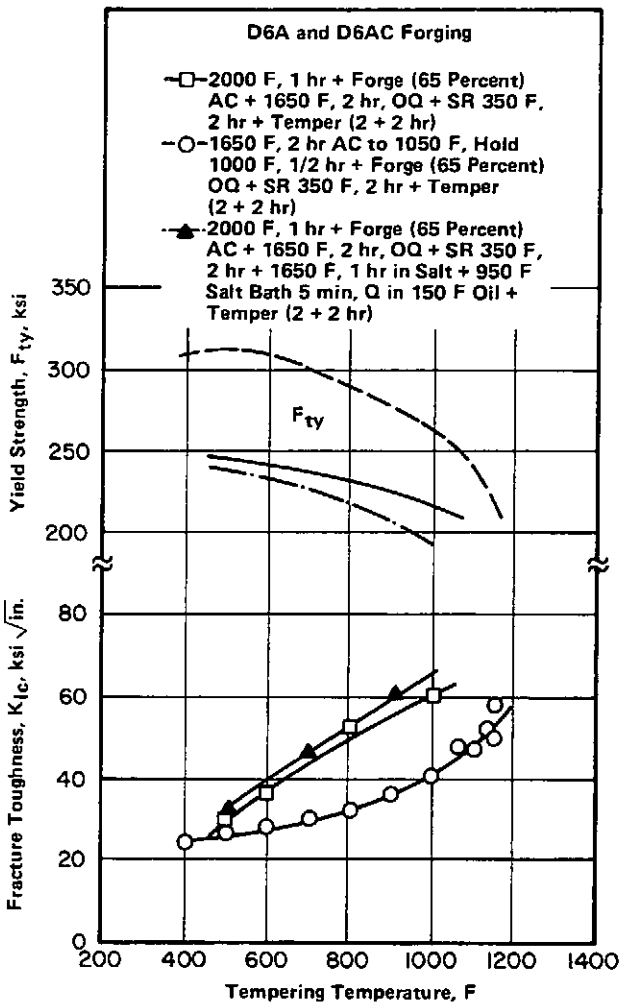

FIGURE 3.027210. EFFECT OF TEMPERING TEMPERATURE ON FRACTURE TOUGHNESS AND YIELD STRENGTH FOR THREE THERMAL-MECHANICAL PROCESSING TREATMENTS OF FORGED ALLOY (42)

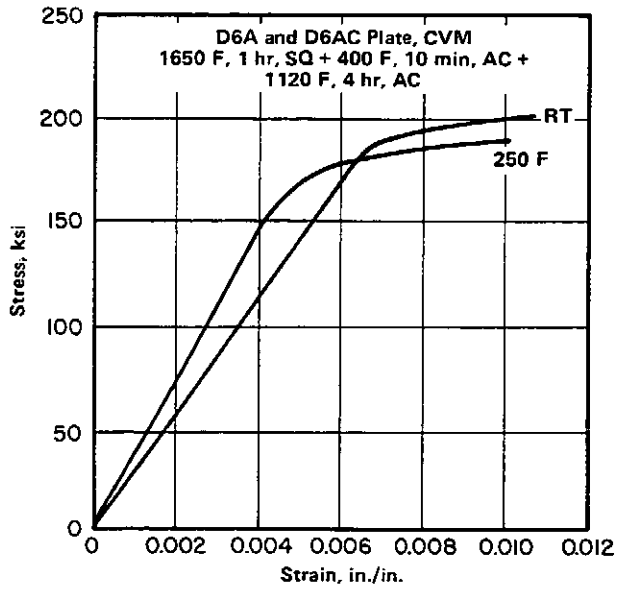

FIGURE 3.0311. STRESS-STRAIN CURVES FOR PLATE AT ROOM TEMPERATURE AND 250 F (5)

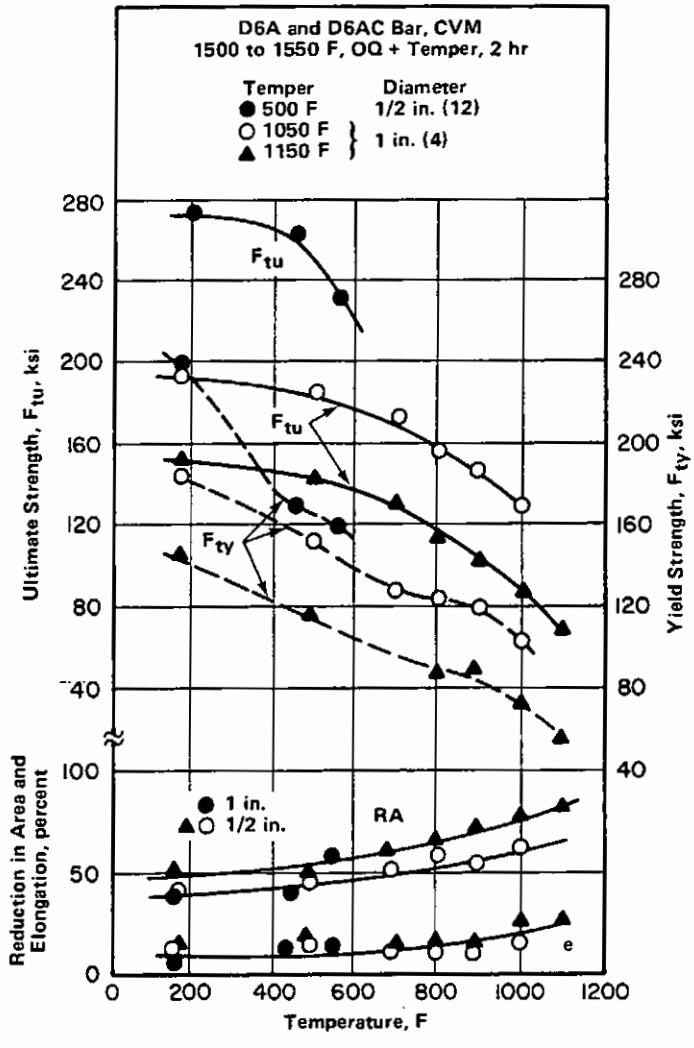

FIGURE 3.0312. EFFECT OF TEST TEMPERATURE ON TENSILE PROPERTIES OF BAR AT SEVERAL STRENGTH LEVELS (4, 12)

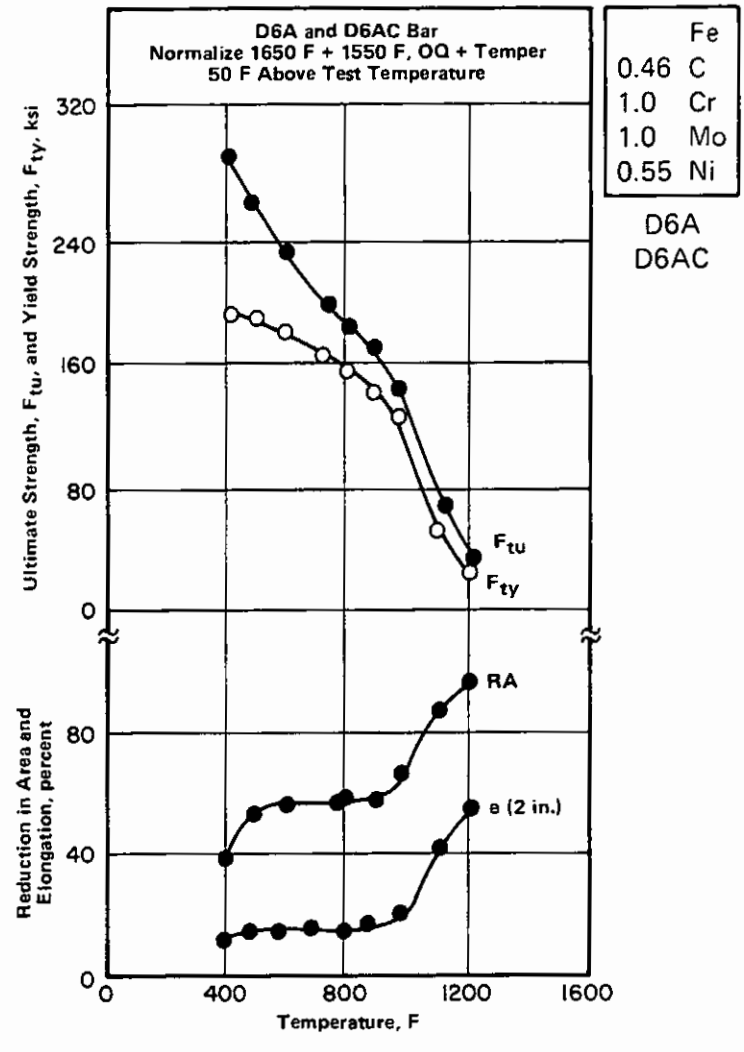

FIGURE 3.0313. EFFECT OF TEST TEMPERATURE ON TENSILE PROPERTIES OF BAR (4)

Alloy	D6A – D6AC			
Form	0.8-in. and 1.5 – 1.8-in. Plate (CVM) – L			
Condition	1650 F or 1700 F + Ausbay Quench to 975 F + Quench in Oil or Salt + Temper at 1000 F to 1025 F, 2 + 2 hr + AC			
Test Temp, F	-40	+35	+70	+175
F_{tu}, ksi	247(a)	241(c)	238(d)	231(c)
F_{ty}, ksi	229(a)	224(c)	217(d)	211(c)
e (1 or 2 in.), percent	11(b)	13(c)	13(e)	15(c)
RA, percent	41(b)	43(c)	45(f)	50(c)

(a) Average of 9.
(b) Average of 5.
(c) Average of 2.
(d) Average of 59.
(e) Average of 36.
(f) Average of 38.

TABLE 3.0314. EFFECT OF TEST TEMPERATURE ON TENSILE PROPERTIES OF PLATE (45)

	Fe
0.46	C
1.0	Cr
1.0	Mo
0.55	Ni

D6A
D6AC

Alloy	D6A – D6AC	
Form	0.8 in. and 1.5 – 1.8 in. Forgings (CVM) – L	
Condition	1650 F or 1700 F + Ausbay Quench to 975 F + Quench in Oil or Salt + Temper at 1000 F to 1025 F, 2 + 2 hr + AC	
Test Temp, F	-40	+70
F_{tu}, ksi	247(a)	233(c)
F_{ty}, ksi	229(a)	214(c)
e (1 or 2 in.), percent	11(b)	13(d)
RA, percent	41(b)	45(d)

(a) Average of 5. (c) Average of 17.
(b) Average of 2. (d) Average of 12.

TABLE 3.0315. EFFECT OF TEST TEMPERATURE ON TENSILE PROPERTIES OF FORGINGS (45)

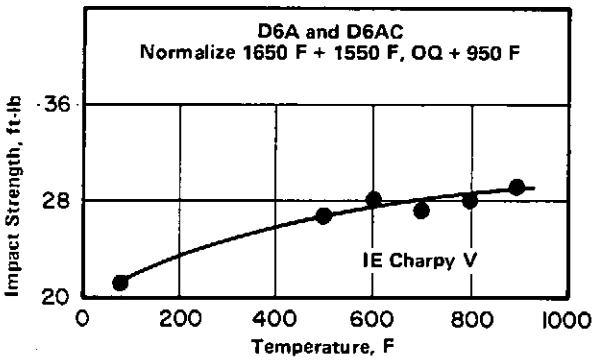

FIGURE 3.0331. ELEVATED TEMPERATURE CHARPY V-NOTCH IMPACT PROPERTIES (4)

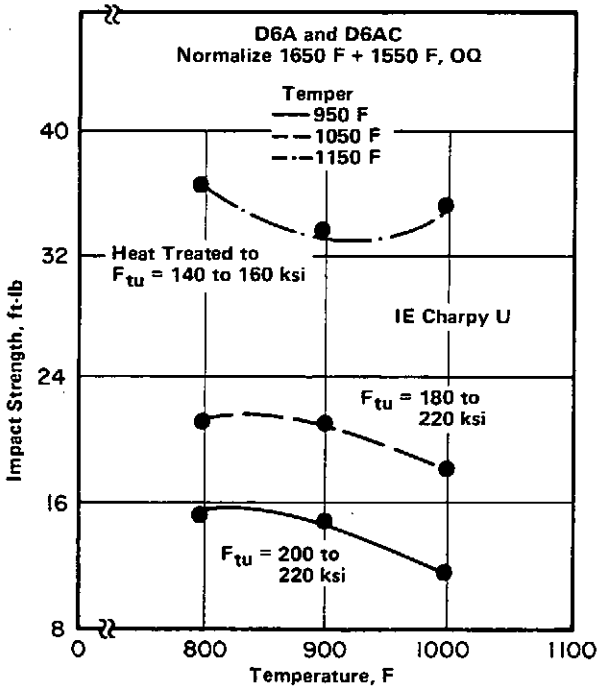

FIGURE 3.0332. ELEVATED TEMPERATURE CHARPY U-NOTCH IMPACT PROPERTIES FOR VARIOUS STRENGTH LEVELS (4)

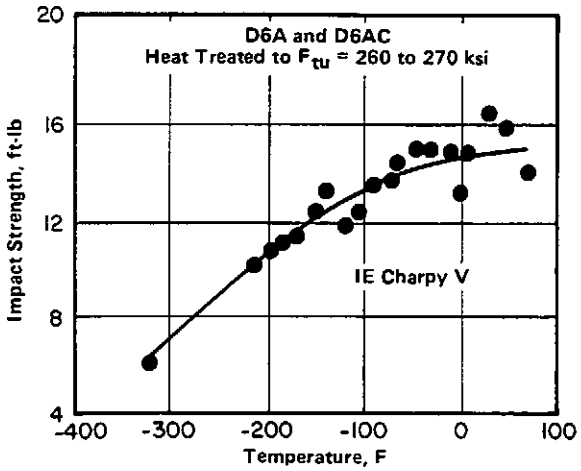

FIGURE 3.0333. LOW TEMPERATURE CHARPY V-NOTCH IMPACT PROPERTIES (4)

	Fe
0.46	C
1.0	Cr
1.0	Mo
0.55	Ni

D6A
D6AC

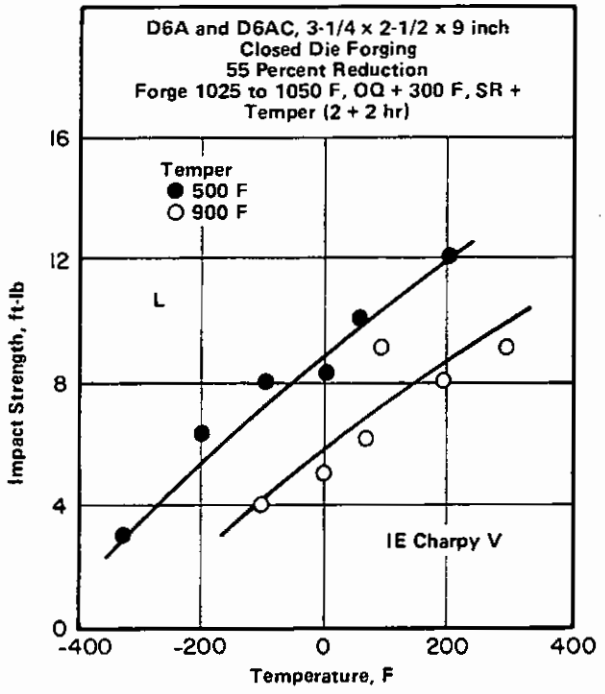

FIGURE 3.0334. EFFECT OF TEST TEMPERATURE ON IMPACT STRENGTH OF A VARIABLE CROSS SECTION AUSFORMED FORGING (10)

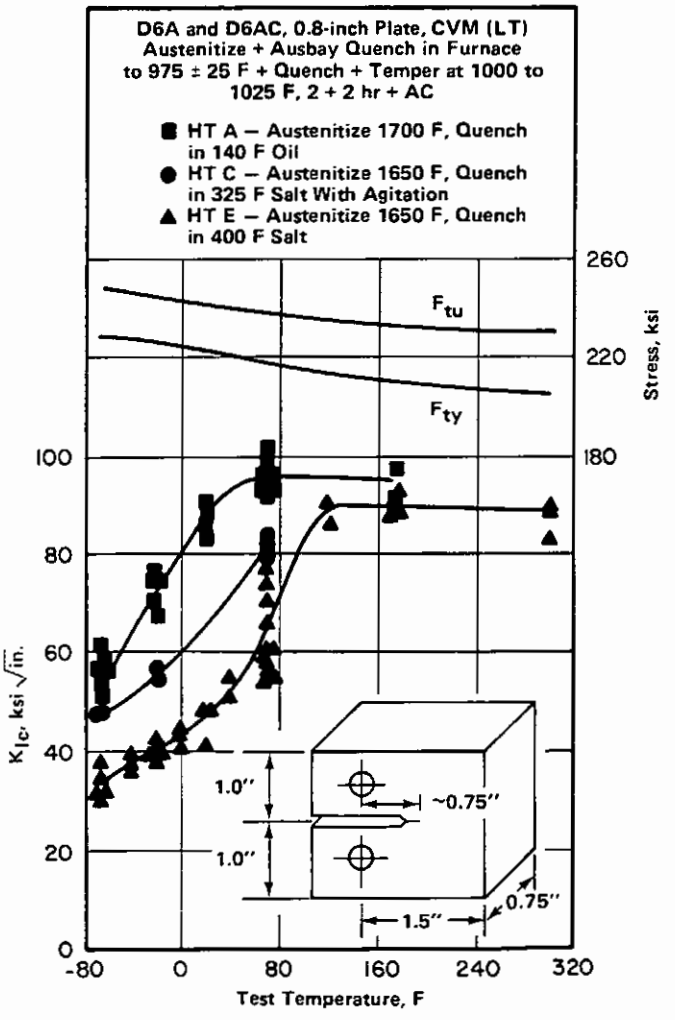

FIGURE 3.03721. EFFECT OF TEST TEMPERATURE ON PLANE STRAIN FRACTURE TOUGHNESS OF 0.8-INCH THICK CVM PLATE (45)

	Fe
0.46	C
1.0	Cr
1.0	Mo
0.55	Ni

D6A
D6AC

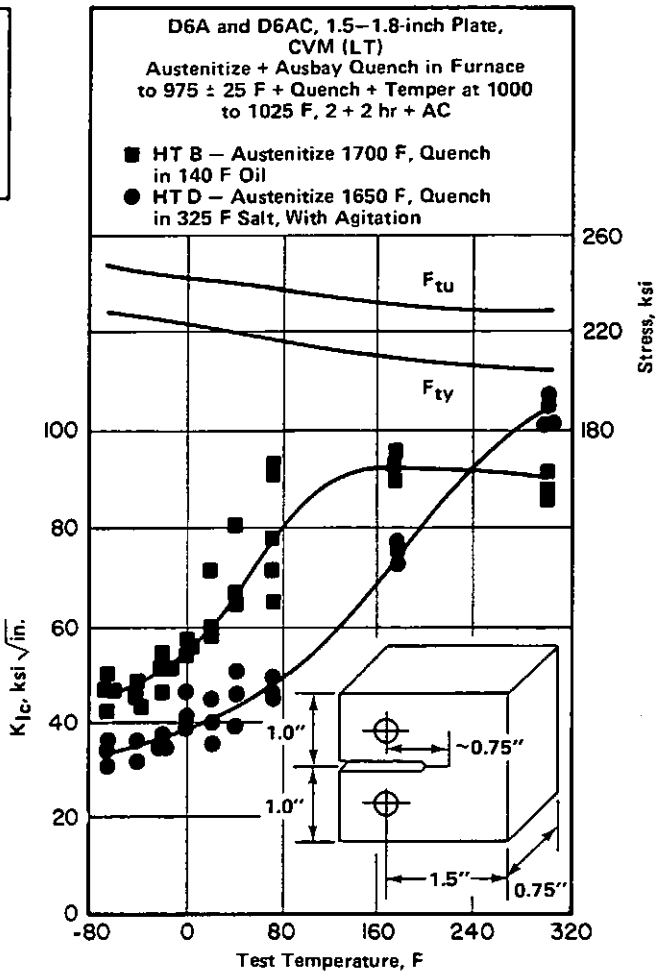

FIGURE 3.03723. EFFECT OF TEST TEMPERATURE ON PLANE STRAIN FRACTURE TOUGHNESS OF CVM FORGINGS (45)

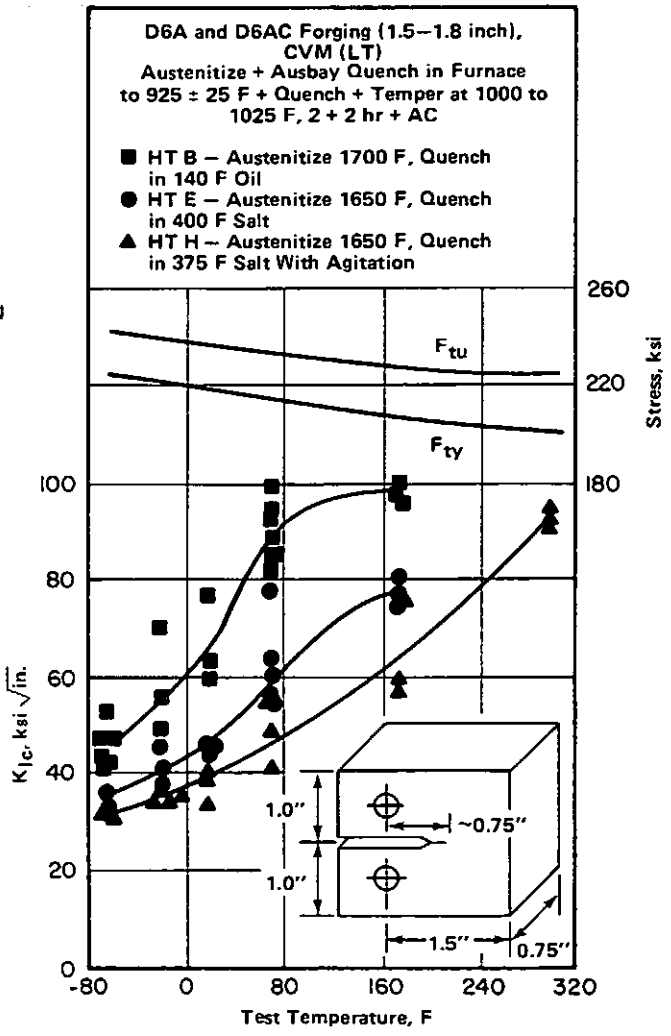

FIGURE 3.03723. EFFECT OF TEST TEMPERATURE ON PLANE STRAIN FRACTURE TOUGHNESS OF CVM FORGINGS (45)

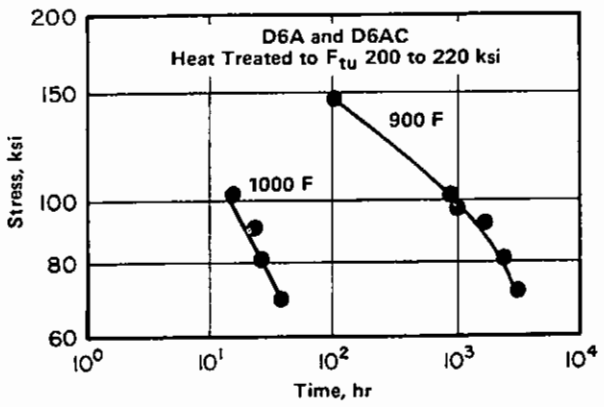

FIGURE 3.041. CREEP-RUPTURE CURVES AT 900 AND 1000 F (4)

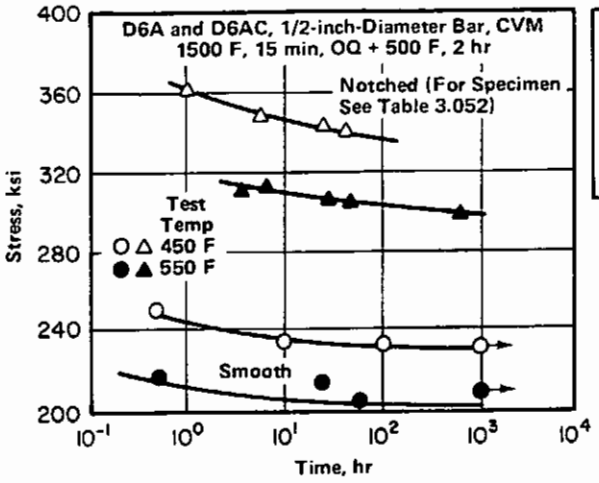

FIGURE 3.042. CREEP-RUPTURE STRENGTH OF SMOOTH AND NOTCHED BAR AT ELEVATED TEMPERATURES (12)

Alloy	D6A – D6AC								
Form	0.125-inch Sheet (CVM)								
Condition	1650 F, AC + 1550 F, OQ + 600 F (2 + 2 hr) + 0.38 percent Strain + 400 F, 2 hr								
	Stress Ratio		Stress Concen-	Fatigue Strength, ksi, at Cycles					
Method	A	R	tration	10^2	10^3	10^4	10^5	10^6	10^7
Direct Stress	1	0	Smooth	270	260	230	125	120	120

TABLE 3.051. FATIGUE STRENGTH OF MARSTRAINED SHEET (11)

Alloy	D6A – D6AC								
Form	1/2-inch Bar								
Condition	1500 F, 15 min, OQ + 500 F, 2 hr								
	Direct Stress Ratio		Stress Concen-	Fatigue Strength, ksi, at Cycles					
Test Temp, F	A	R	tration	10^2	10^3	10^4	10^5	10^6	10^7
RT	1	0	Smooth	–	270	230	170	150	150
	∞	-1		220	180	160	130	100	100
450	1	0	Smooth	–	260	220	170	150	135
	∞	-1		220	180	160	130	100	90
550	1	0	Smooth	–	240	215	170	150	130
	∞	-1		220	180	140	110	85	75
RT	1	0	Notched	300	190	120	80	80	80
	∞	-1		200	135	65	50	50	50
450	1	0	Notched	–	–	100	85	70	60
	∞	-1		–	–	–	45	40	40
550	1	0	Notched	280	140	100	80	65	55
	∞	-1		170	100	65	50	45	40

Notched Specimen

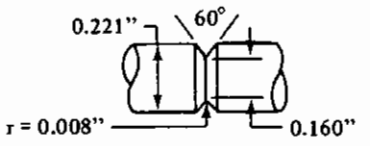

$K_t = 3.00$

TABLE 3.052. EFFECT OF TEST TEMPERATURE ON SMOOTH AND NOTCHED FATIGUE PROPERTIES OF BAR (12)

	Fe
0.46	C
1.0	Cr
1.0	Mo
0.55	Ni

D6A
D6AC

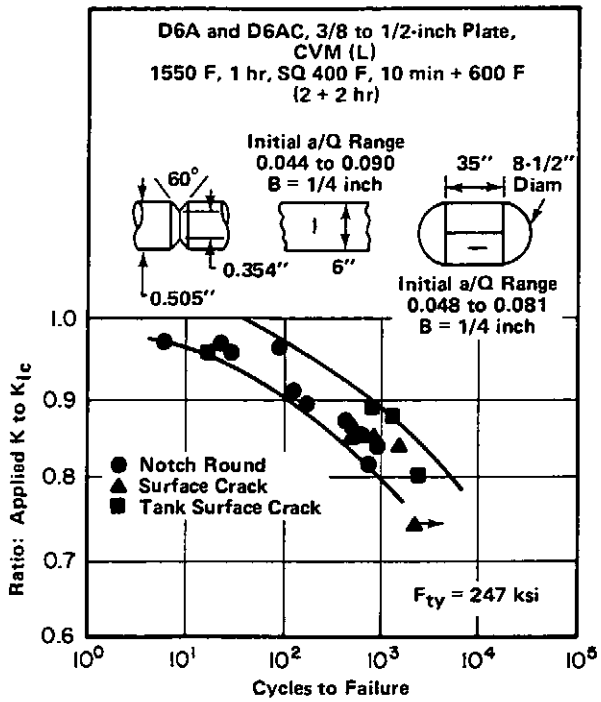

FIGURE 3.053. LOW CYCLE FATIGUE BEHAVIOR OF CRACKED PLATE SPECIMENS AND TANKS (18)

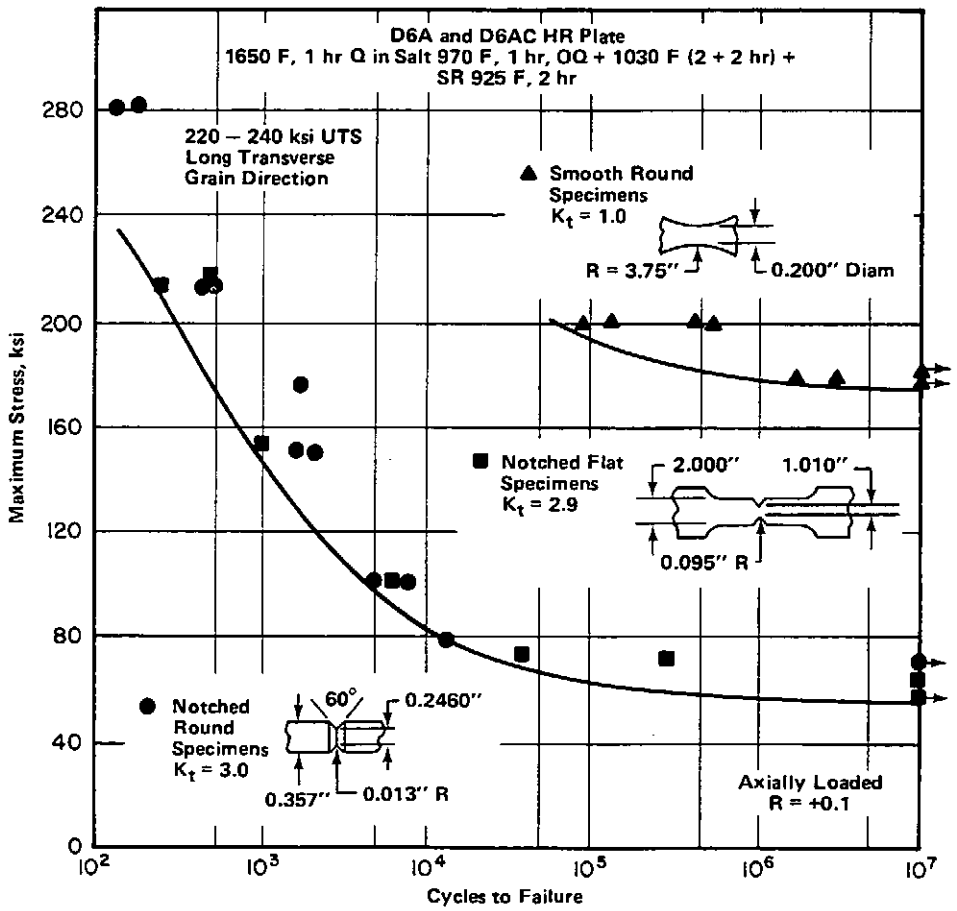

FIGURE 3.054. S-N CURVES FOR 220 TO 240 KSI HOT ROLLED PLATE (44)

	Fe
0.46	C
1.0	Cr
1.0	Mo
0.55	Ni

D6A
D6AC

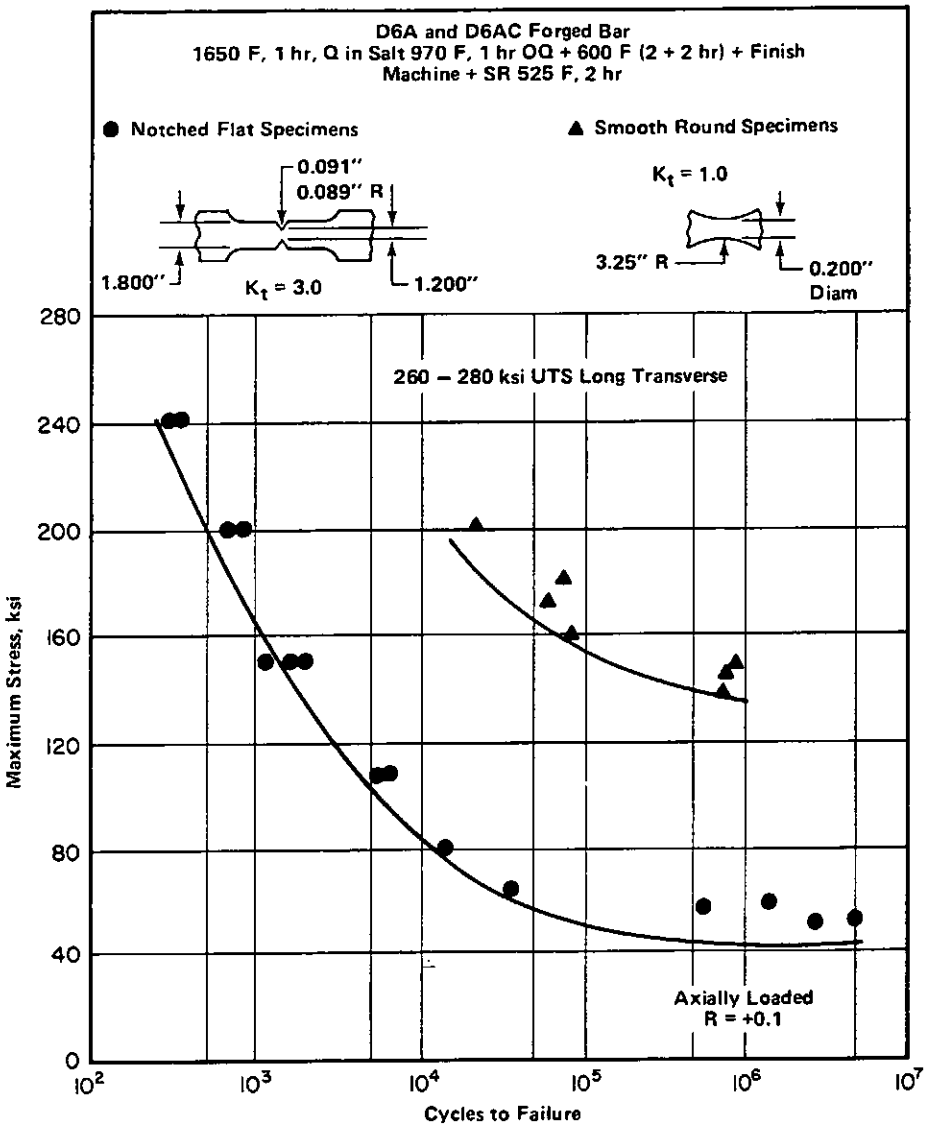

FIGURE 3.055. S-N CURVES FOR 260 TO 280 KSI FORGED BAR (44)

	Fe
0.46	C
1.0	Cr
1.0	Mo
0.55	Ni

D6A
D6AC

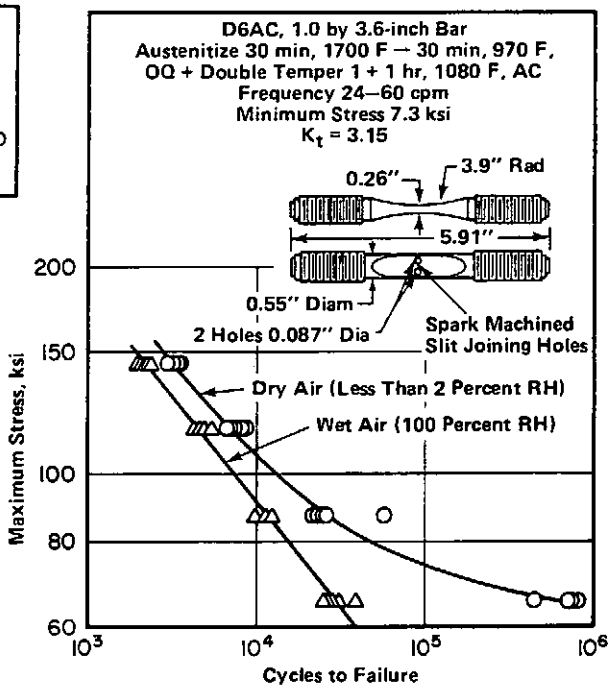

FIGURE 3.056. EFFECTS OF HUMIDITY ON FATIGUE BEHAVIOR OF KEYHOLE NOTCHED BAR AT 95 F (67)

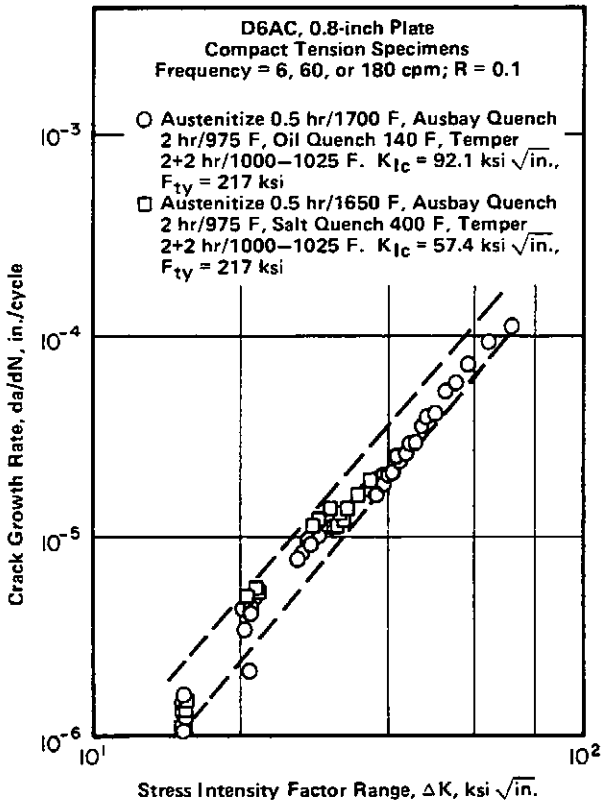

FIGURE 3.059. FATIGUE CRACK-GROWTH RATES FOR HIGH AND MEDIUM TOUGHNESS PLATE IN DESICCATED AIR AT ROOM TEMPERATURE (45)

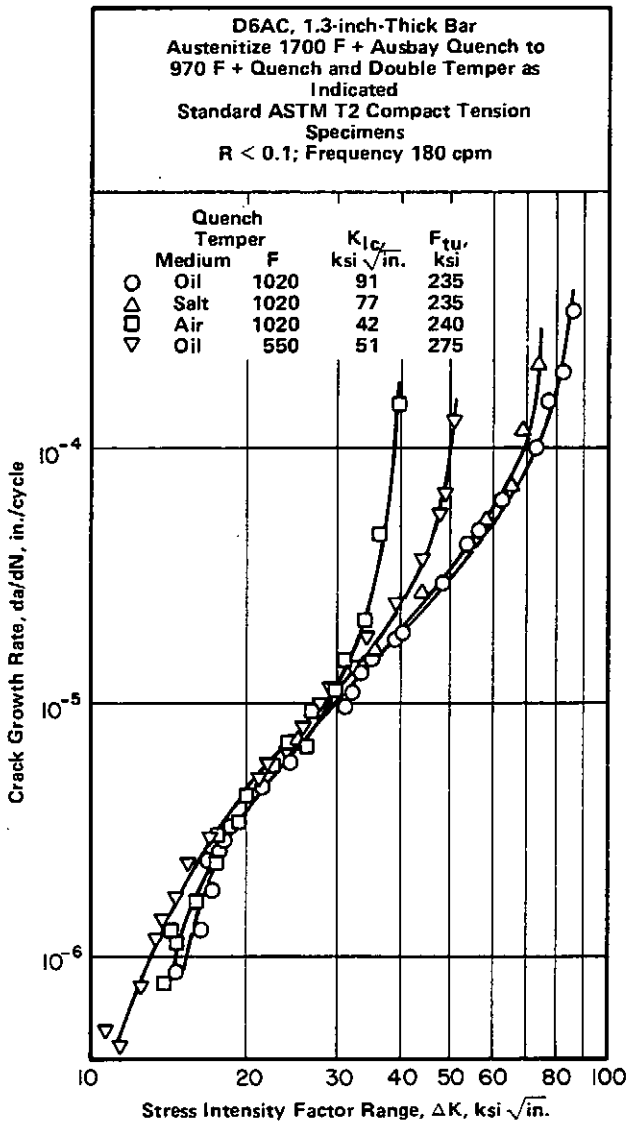

FIGURE 3.058. EFFECTS OF QUENCHING ON FATIGUE CRACK-GROWTH BEHAVIOR IN DRY AIR AT ROOM TEMPERATURE (68, 69)

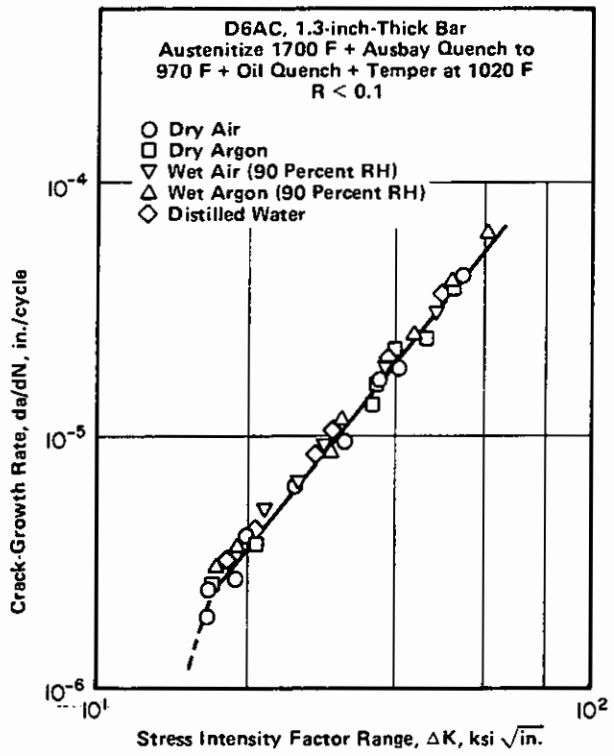

(a) Frequency 600 Cycles/Minute

FIGURE 3.0511. EFFECTS OF HUMIDITY AND FREQUENCY ON FATIGUE CRACK-GROWTH BEHAVIOR AT ROOM TEMPERATURE (68, 69)

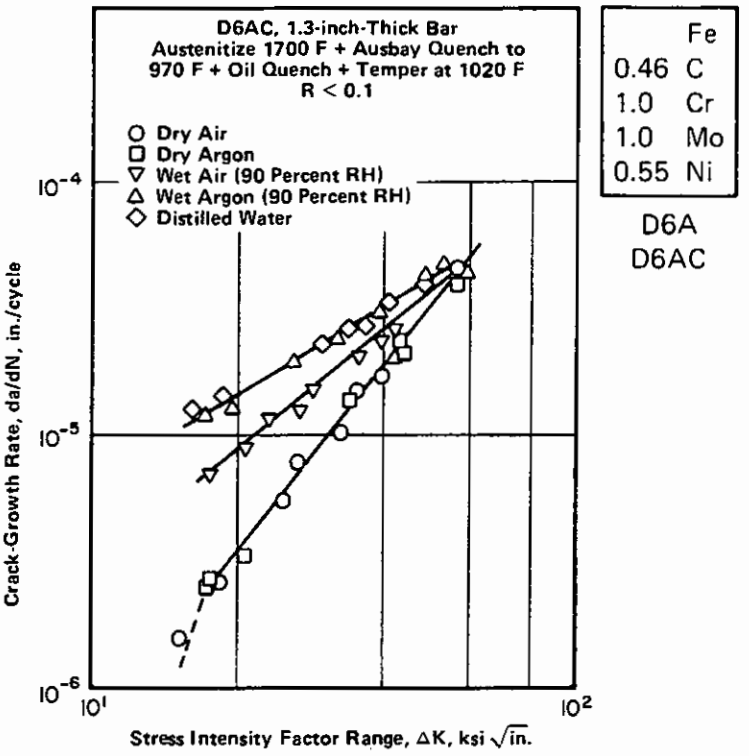

(b) Frequency 60 Cycles/Minute

FIGURE 3.0511. EFFECTS OF HUMIDITY AND FREQUENCY ON FATIGUE CRACK-GROWTH BEHAVIOR AT ROOM TEMPERATURE (68, 69)

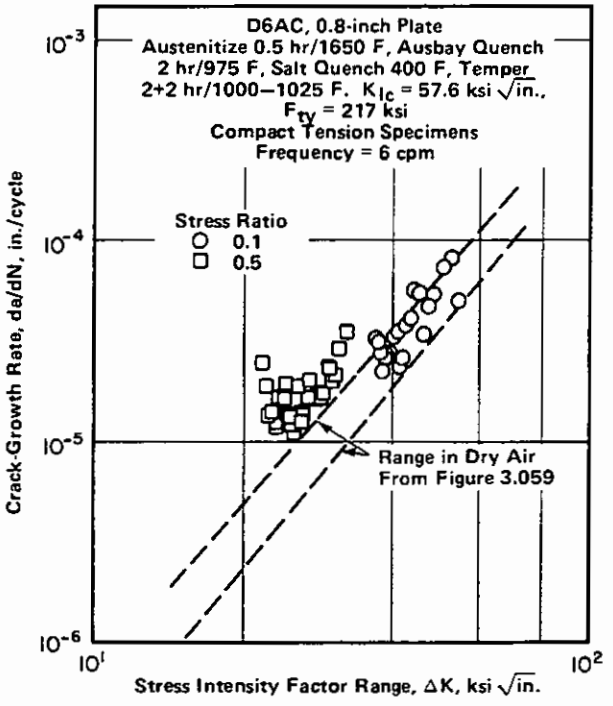

FIGURE 3.0512. FATIGUE CRACK-GROWTH RATES FOR MEDIUM TOUGHNESS PLATE IN LABORATORY AIR (50 TO 70 PERCENT RH) AT ROOM TEMPERATURE (45)

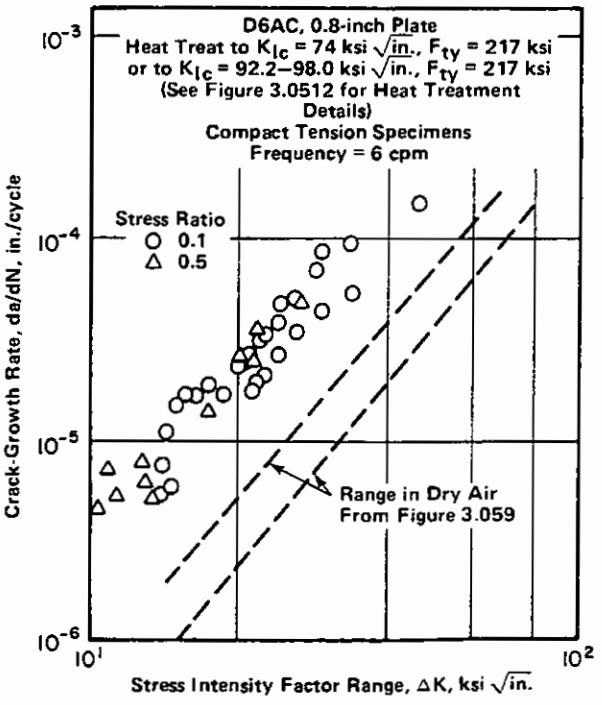

FIGURE 3.0513. FATIGUE CRACK-GROWTH RATES FOR HIGH AND MEDIUM TOUGHNESS PLATE IN DISTILLED WATER AT ROOM TEMPERATURE (45)

	Fe
0.46	C
1.0	Cr
1.0	Mo
0.55	Ni

D6A
D6AC

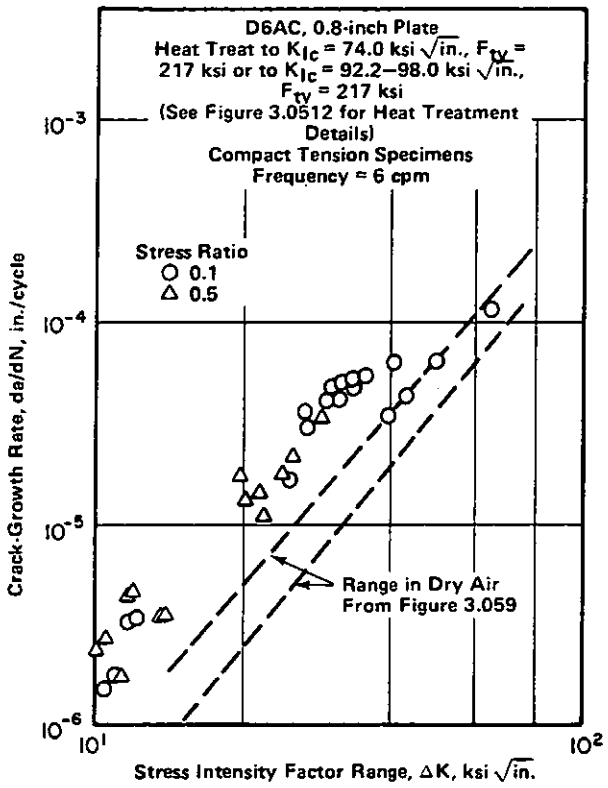

FIGURE 3.0514. FATIGUE CRACK-GROWTH RATES FOR HIGH AND MEDIUM TOUGHNESS PLATE IN WATER-SATURATED JP-4 FUEL AT ROOM TEMPERATURE (45)

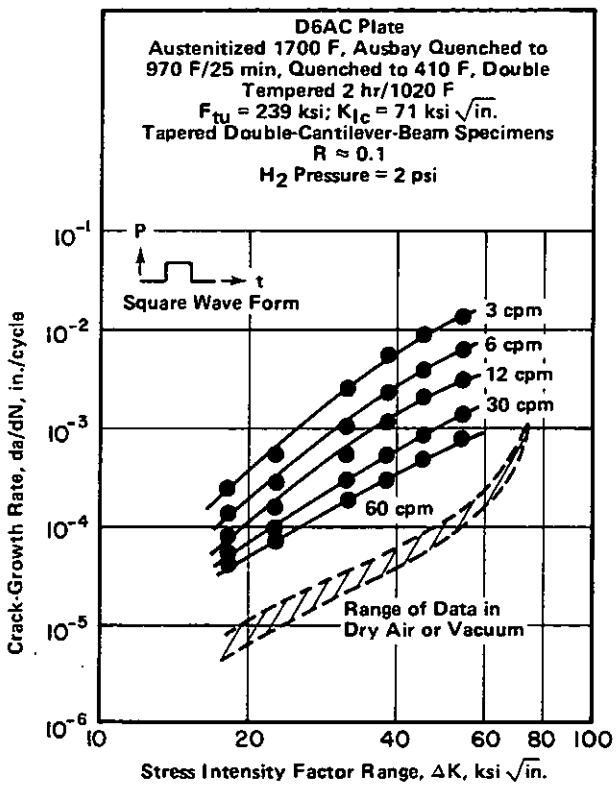

FIGURE 3.0516. EFFECTS OF CYCLIC FREQUENCY ON FATIGUE CRACK-GROWTH BEHAVIOR IN HYDROGEN WITH COMPARISON TO AIR AND VACUUM (65)

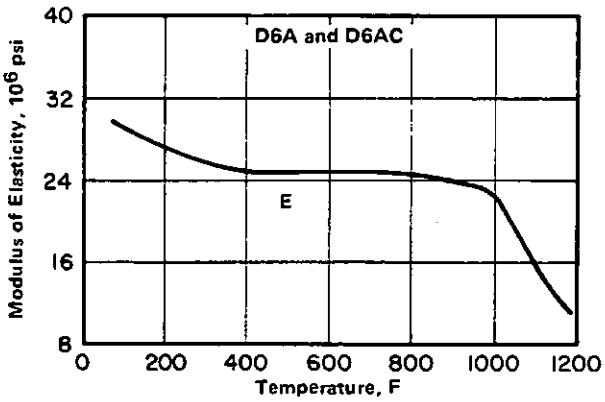

FIGURE 3.0621. MODULUS OF ELASTICITY AT ROOM AND ELEVATED TEMPERATURES (4)

Fe
0.46 C
1.0 Cr
1.0 Mo
0.55 Ni

D6A
D6AC

Alloy	D6A – D6AC	
Thickness, in.	0.1 to 0.375	
GTA Weld	Primary (5)	Weld Repair After HT (22)
Temperature Preheat and Interpass	500 to 650 F	500 to 650 F
Postheat	(a, b)	650 to 700 F, 2 hr, AC to 150 to 175 F + 650 F to 700 F, 1 hr, AC
Stress Relief	1200 to 1250 F(b)	1100 F, 1 hr, AC
Heat Treatment	1650 F, 1 hr, SQ 400 F 10 min, AC + 400 F, 1 hr AC + 1075 F, 4 hr, AC (F_{ty} = 215 ksi)	1650 F, 2 hr, FC to 1600 F 30 min, SQ 400 F, 10 min, AC + 400 F, 2 hr AC + 1125 F, 4 hr, AC (F_{ty} = 180 ksi)

(a) For highly restrained sections, Ref. 4 gives 575 to 625 F, 1.5 hr, AC to 300 F as soon after welding as possible followed by immediate stress relief.

(b) For welded tank fabrications (0.2 to 1.0-inch sections), Ref. 5, stress relief before part has cooled below interpass temperature.

TABLE 4.0311. RECOMMENDED WELD HEAT TREAT SEQUENCE FOR PRIMARY WELDS AND WELD REPAIR AFTER HEAT TREATMENT (5, 22)

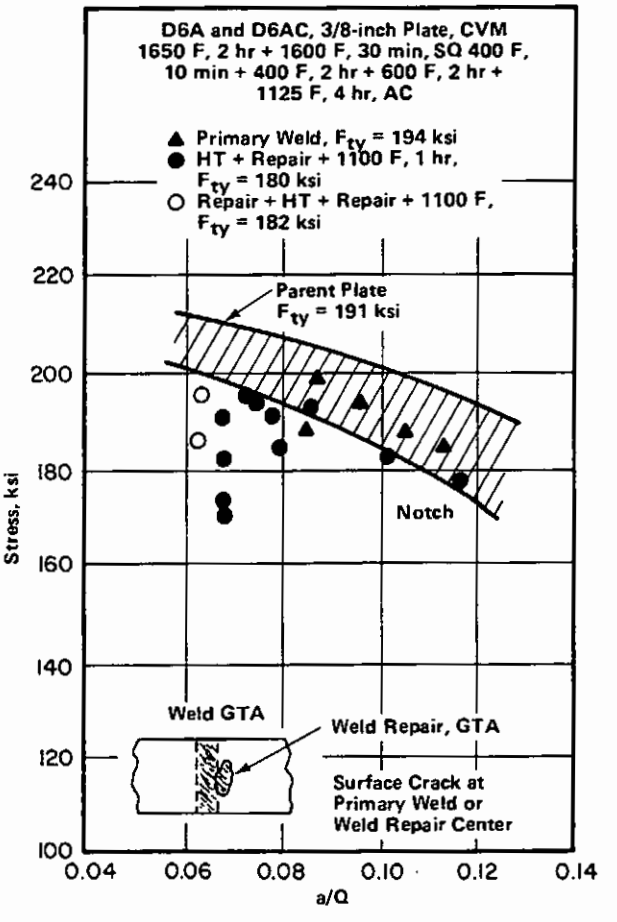

FIGURE 4.0312. EFFECT OF SURFACE CRACK SIZE ON SHARP NOTCH STRENGTH OF PRIMARY WELDS AND WELD REPAIRS MADE AFTER HEAT TREATMENT (22)

	Fe
0.46	C
1.0	Cr
1.0	Mo
0.55	Ni

D6A
D6AC

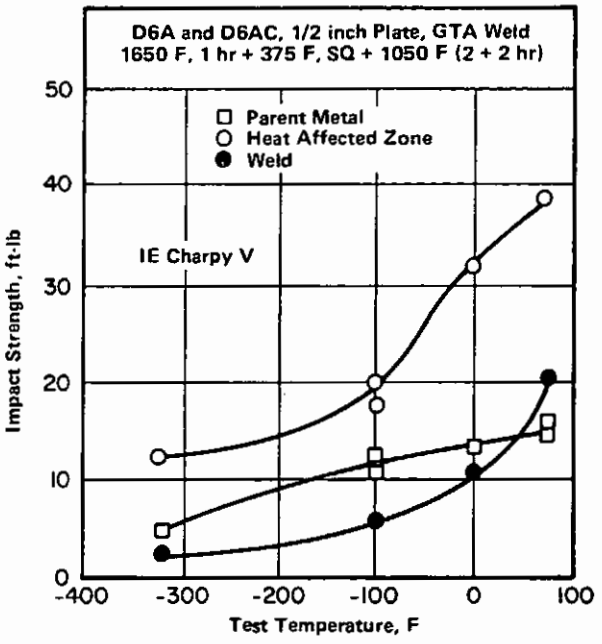

FIGURE 4.0313. EFFECT OF WELDING ON LOW TEMPERATURE CHARPY V IMPACT PROPERTIES (39)

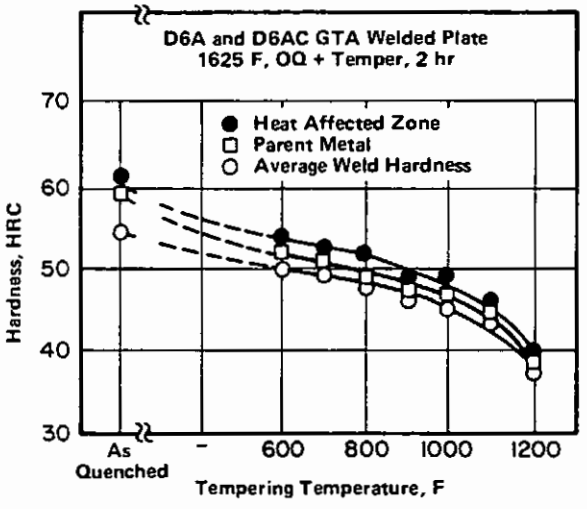

FIGURE 4.0314. HARDNESS SURVEY ON WELDED PLATE (30)